

AD-A089 631

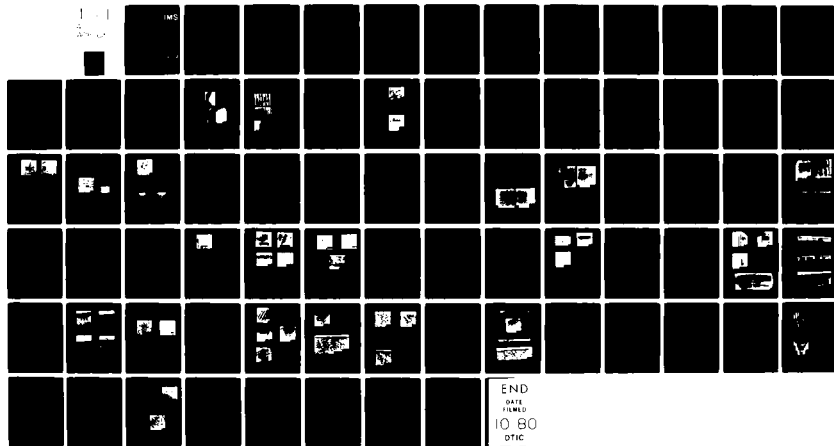
CONNECTICUT UNIV STORRS INST OF MATERIALS SCIENCE  
ELECTRON BEAM/LASER GLAZING OF IRON-BASE MATERIALS.(U)  
JUL 80 P R STRUTT

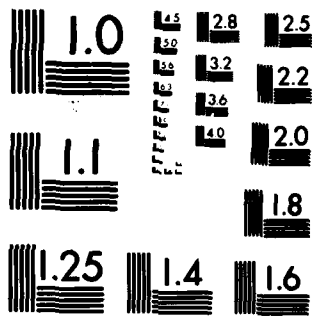
F/G 20/7

N00014-78-C-0580

NL

UNCLASSIFIED





MICROCOPY RESOLUTION TEST CHART  
NATIONAL BUREAU OF STANDARDS-1963-A

AD A089631

406716  
↓

LEVEL

①  
SC

IMS

INSTITUTE OF MATERIALS SCIENCE

1173

DTIC  
ELECTE  
SEP 29 1980  
S D  
A

DDC FILE COPY

DISTRIBUTION STATEMENT A  
Approved for public release;  
Distribution Unlimited

THE UNIVERSITY OF CONNECTICUT  
Storrs - Connecticut

80 9 26 007

Electron Beam/Laser Glazing of  
Iron-Base Materials

P. R. Strutt

July 1980

Annual Progress Report

Office of Naval Research  
Arlington, Virginia 22217  
Contract #N00014-78-C-0580

DTIC  
ELECTE  
SEP 29 1980  
S D  
A

DISTRIBUTION STATEMENT A  
Approved for public release;  
Distribution Unlimited

**Electron Beam/Laser Glazing of  
Iron-Base Materials**

**P. R. Strutt**

**July 1980**

**Annual Progress Report**

**Office of Naval Research  
Arlington, Virginia 22217**

**Contract #N00014-78-C-0580**

**Reproduction in whole or in part is permitted for  
any purpose of the United States Government**

**Distribution of this document is unlimited.**

**Metallurgy Department  
Institute of Materials Science  
University of Connecticut  
Storrs, Connecticut 06268**

Accession For	
Doc. #	<input checked="checked" type="checkbox"/>
Doc. #13	<input type="checkbox"/>
Unprocessed	<input type="checkbox"/>
Justification	
By	
Distribution/	
Availability Code	
Dist	Avail and/or special
A	

## CONTENTS

Introduction	(i)
<u>SECTION I</u>	
E.B. Surface Glazing Facility	1
Formation of Rapidly Quenched Surface Layers by E.B. Scanning	4
<u>SECTION II</u>	
Conference Papers presented	14
(i) Laser and E.B. Melting of Fe-Based Hard Materials	15
(ii) Microstructural Control by E.B. Surface Melting	24
(iii) Electron Beam Glazed Surface Areas	34
<u>SECTION III</u>	
Electron-Beam Glazed Surface Areas - Wear Studies	40
<u>SECTION IV</u>	
Elevation and Depression of the $M_s$ Temperature by Laser and E.B. Glazing of a High Carbon-Low Alloy Steel	57

## Introduction

The capability of producing a uniform rapidly solidified layer of relatively large area on a substrate material has been clearly demonstrated during the period covered by this report. This together with a detailed microstructural characterization of rapidly solidified hard iron-base alloys and preliminary wear studies is discussed in the following sections. The report on O.N.R. contract N00014-79-C0580 is for the period 30 June 1979 to 30 June 1980.

The electronic circuitry used in the electron beam pattern generator was entirely designed in the Institute of Materials Science by Mr. Gary Moebus in consultation with Professor Strutt and Dr. Lewis. Further design work for obtaining scanning patterns over larger areas at a lower distortion level is continuing. A summary of the electron beam surface glazing facility is included in Section I (pp.1-3). A paper describing the parameters used for obtaining rapidly quenched surface layers is also included in this section (pp.4-13).

Papers to appear in conference proceedings on the microstructure & topography of rapidly solidified layers of several hard iron-base materials are included in Section II. This work was performed by Dr. B.G. Lewis and Mr. D.G. Gilbert, these workers also initiated combined sliding/impact wear studies on the same materials which are described in Section III. The hard materials include M2 tool steel and various materials containing  $\approx$  35% volume fraction of titanium carbide particles. The matrix-phase of these materials itself is a highly alloyed steel which is either of the martensitic or maraging type.

Another particularly intriguing aspect of the program is a basic study of the effect of both laser and electron beam glazing a high carbon - low alloy steel. Rather unexpectedly, it was found that these two directed energy sources appeared to produce material with, in some cases, markedly different microstructural characteristics. The results themselves are consistently interpreted on the basis of the nucleation of martensite by either small oxide particle inclusions or a fine dispersion of carbide particles. This work, performed by Mr. Mohan Kurup, forms the basis of his M.S. degree thesis.

A further interim report on M2 tool steel will be circulated in the near future. Work is continuing on the fundamental aspects of rapidly solidified M2 tool steel and we are awaiting the results of recently undertaken compositional mapping of the M2 glazed zones.

SECTION I

## The Electron-Beam Surface Glazing Facility

The Carl Ziess used electron beam welding unit which was acquired during the first two years of the present O.N.R. Contract has been completely re-built so as to be capable of producing high quality "glazed" surface areas on a substrate material. The new features include:

### I. Electron Beam Pattern Generator

Specially designed integrated electronic circuitry has been designed, tested, and made for magnetically deflecting the beam in various modes which include:

#### (i) Rectangular Lissajou Type Patterns

A surface area is swept out by scanning the beam in a pattern produced by applying two nearly equal frequency triangular waveform voltages to the X and Y beam deflection coils. With the present unit both the frequency and difference in frequency between the two signals can be varied independently. The signal voltage applied to the Y-axis deflection coils is selected from one of the following frequencies, 1000, 500, 250, 125, 62.5, 31.25, 15.63, 7.81, 3.91, 1.95 hertz. That applied to the X-axis deflection coils is obtained by multiplying this selected frequency by a factor slightly exceeding unity. The multiplying factor (as determined from a set of quartz crystal oscillators) may be either 1.001, 1.0025, 1.005, 1.010, and 1.015. With the degree of precision and variability attainable it is possible to obtain highly regular electron beam glazed surface areas. Full details of these together with the microstructures on surface to topographic aspects are given in this report in the paper on "Formation of Rapidly Quenched Surface Layers by Electron Beam Scanning".

#### (ii) Single Line Scan Mode

Another type of beam scanning mode is that employed in the familiar television raster where a high speed line velocity is combined with a slower

velocity frame velocity. This mode may be selected in the "beam pattern generator" where the requisite high and low frequency "ramp" signals in the line/frame mode are derived from the range of standard frequencies already mentioned.

(iii) Single Line Scan Mode

In this mode a "ramp" voltage signal is applied to the X or Y axis deflection coils so as to produce a single sweep of the beam across the specimen surface. By knowing the sweep length and transit time the beam velocity is determined. Since the "ramp" frequency may be varied over a large range a corresponding range of beam velocities may also be obtained. This feature is used in parametric studies for determining the effect of beam velocity on melt zone geometry, for instance.

(iv) Cycle Counter and Other Features

An integrated circuit frequency counter is used to count the number of cycles of repetitive beam deflection cycles until a predetermined number has been attained; the preselected number may be 1 to 9999. Once the counter reaches this number the beam returns to an origin which may be selected to be outside the region surface melted by the scanning beam. This counting capability is used in parametric studies for determining the effect of successively melting and quenching any desired number of times or of examining the effect of overlapping adjacent "glazed" traces in surface layers formed by the scanning modes previously cited.

II. Mechanical Beam/Specimen Motion

A mechanical rotational stage has been constructed for moving the specimen relative to the beam over a wide range of velocities with minimal vibration or jerkiness. The drive for this turntable arrangement is provided by a numerical control motor with constant torque and velocity at any selected

setting. This motor is mounted externally and the motion to the specimen vacuum chamber is through a high speed rotary magnetic fluid seal. The motor controller can be adjusted to any desired number of revolutions/minutes ranging from 0 to 400  $\text{cm.s}^{-1}$ .

### III. Vacuum System

A new vacuum system has been installed with electromagnetic control valves, readily connectable/disconnectable joints for maintenance, and a vacuum system gauge monitor. With this system a vacuum of  $\sim 10^{-5}$  mm is used in the actual surface glazing experiments.

### Formation of Rapidly Quenched Surface Layers by Electron Beam Scanning

The intriguing metallurgical structures produced by laser and electron beam glazing (1-6) create considerable interest in developing a convenient method for glazing the entire surface of a substrate material. In this respect electron beam glazing is admirably suitable since the beam may be rapidly deflected over the surface area by electromagnetic beam deflection coils. Following previously reported electron beam surface scanning experiments (7-9) the present paper will show that a beam scanning mode employed for generalized surface heating (10) may also be used for producing well controlled surface glazing. With the degree of precision control attainable with electronic circuiting now available, the electron beam scanning technique may be used for obtaining high quality smooth surfaces on a M2 tool steel substrate.

The type of scanning pattern used is obtained by applying two nearly equal frequency triangular waveform signals to the X and Y axis beam deflection coils of the electron beam surface melting unit. The succession of rectangular Lissajous figures traced out in this scanning mode are shown in Fig. 1, where X and Y axis deflection of the spot on the substrate has maximum value of a and b respectively. The rectangular path results from the progressive amount of phase lag of the Y-axis signal behind the X-axis signal. As the beam sweeps diagonally across from A (where the phase difference is zero) the path intercepts BC when the X-axis signal attains its maximum amplitude, the intersection point is at a distance  $b(\frac{\Delta f}{f})/(1+\frac{\Delta f}{f})$  below C. Following this, the path next intercepts CD when the Y-axis signal attains its maximum value. The distance of this intercept point to the left of C is  $a(\frac{\Delta f}{f})$ . In proceeding with this simple analysis it is readily apparent how the successive rectangular type of scanning pattern is obtained.

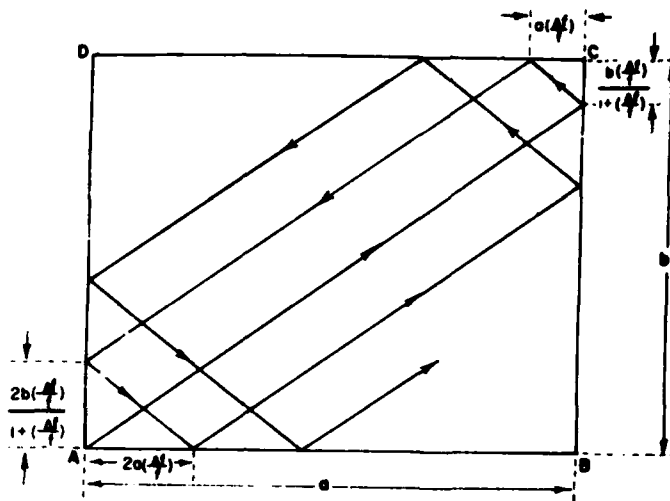


Figure 1: Schematic diagram showing the succession of rectangular Lissajous traced out during electron-beam scanning.

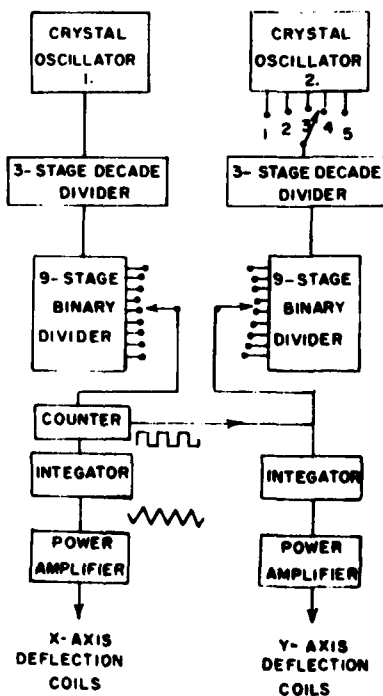


Figure 2: Block diagram illustrating the method for obtaining frequencies  $f$  and  $f + \Delta f$ .

Simple consideration shows that the angle  $\theta$  in Fig. 1 is given by Eqn. 1

$$\tan \theta = \frac{b}{a} \cdot \frac{1}{(1 + \Delta f/f)} ; \text{-----}(1).$$

Also by geometrical construction the spacing  $d$  between two adjacent diagonal traces is given by Eqn. 2. It should be noted at this juncture that no mention has been made of the actual beam spot diameter ( $w$ ). When considering a beam of finite width the diagonal lines in the pattern will represent the path traced out by the center of the spot.

$$d = \frac{2ab(\frac{\Delta f}{f})}{\sqrt{a^2(1 + \frac{\Delta f}{f})^2 + b^2}} ; \text{-----}(2).$$

In considering the  $n^{\text{th}}$  cycle, the beam path intercept on BC is a distance  $y_n$  away from C, see Eqn. 3.

$$y_n = \frac{(2n - 1)(\frac{\Delta f}{f}) \cdot b}{(1 + \frac{\Delta f}{f})} ; \text{-----}(3).$$

Equation 3 may be used to find  $n$ , the number of cycles required to sweep out the entire area ABCD, simply by noting that  $y_n$  will then be equal (or about equal) to  $b$ . The precise condition is given by Eqn. 4.

$$n \geq 1/2(\frac{\Delta f}{f}) > (n - 1) ; \text{-----}(4).$$

It should be noted that although the time to complete a frame is  $(n/f)$  the line spacing is frequency independent and depends on the ratio  $(\Delta f/f)$ .

The block diagram in Fig. 2 illustrates the method for obtaining the two closely related frequencies  $f$  and  $f + \Delta f$ . In each channel a quartz crystal oscillator ( $\sim 1$  megahertz) produces a square waveform voltage signal. This is first divided in three steps to produce a signal in the kilohertz range and then subsequently divided by a cascade of nine binary dividers. Any particular pair of frequencies may be selected for producing the actual signals applied to the beam deflection coils. The frequencies of the master quartz

crystals in the right-hand channel range from 1.001 to 1.015 that of the left hand side; there are thus five possible choices of  $(\Delta f/f)$ . Another important feature is the pulse counter which may be set to control the actual number of cycles from one to 9999. Finally, the integrator circuits are used to transform the signals from a square to a triangular waveform. Following power amplification these signals are applied to the beam deflection coils.

In the experiments to be described the tool steel M2 was used as a standard substrate material since its laser/electron beam glazing characteristics are established (11, 12). An accelerating voltage of 75kV was used to produce a 375 watt beam power and the beam diameter was 0.5 mm. The conditions used for glazing 7 rectangular blocks (5 cm x 5 cm x 1 cm) of M2 tool steel are given in Table I; the dimensions of the glazed area are 2.5 cm x 2.0 cm. Low magnification micrographs of regions glazed for  $f$  equal to 60 hertz are shown in Fig. 3, where Fig. 3a shows part of successive glazed traces obtained for  $\frac{\Delta f}{f}$  equal to 1/150. With this value of  $(\Delta f/f)$  the number of cycles frame is 75 and the surface finish obtained after a complete frame is shown in Fig. 3b. As evident from Table I and Eqn. 2 the effect of decreasing the ratio  $(\Delta f/f)$  is to reduce the spacing distance  $d$  and as a result produce overlapping of melting zones when  $w > d$ , where  $w$  is the beam diameter. An intriguing finding is the remarkable increase in surface uniformity as  $(\Delta f/f)$  is progressively decreased. This became strikingly evident by comparing Figs. 3b, c, and d where the corresponding values of  $(\Delta f/f)$  are 1/150, 1/450, and 1/600; in each case the value of  $f$  is 60 hertz. The experimental and calculated values of  $d$  are given in Table I for results obtained both at 30 and 60 hertz. Figures 4a, b, and c show the surface topographies of the specimens corresponding to Figs. 3b, c, and d at a higher magnification. At even higher

Table I

f (hertz)	$(\frac{\Delta f}{f})$	n	d ( $\mu$ m)	
			Calculated	Observed
60	1/150	15	207	217
60	1/150	75	207	217
60	1/450	225	69	78
60	1/600	300	52	55
30	1/75	38	413	435
30	1/175	88	178	192
30	1/350	175	112	104

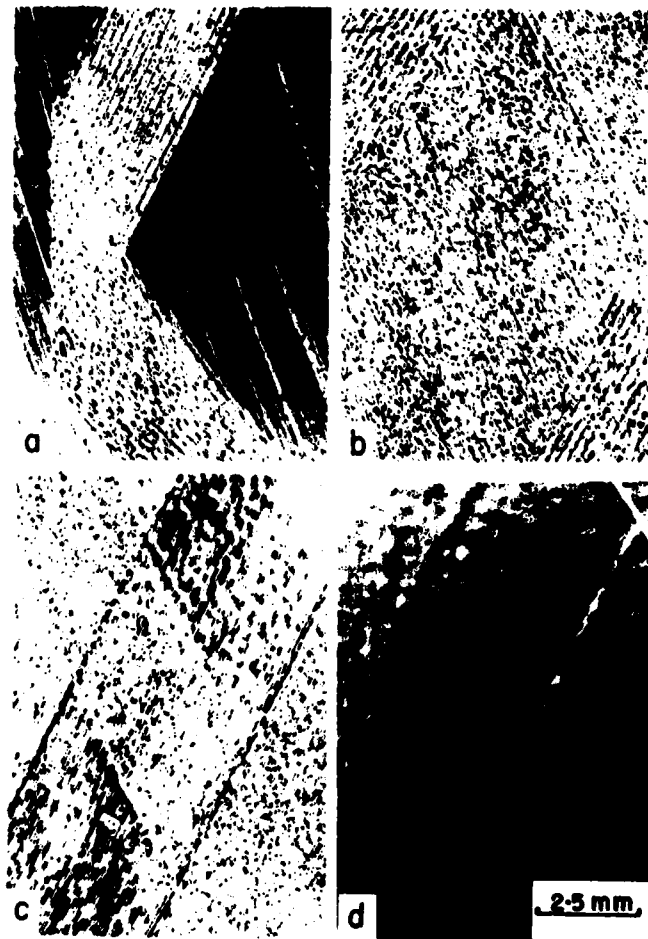


Figure 3: Low magnification micrographs of glazed regions using  $f = 60$  hertz.

- (a) Part of successive glazed traces with  $\Delta f/f = 1/150$
- (b) Surface finish after complete frame. ( $\Delta f/f = 1/150$ )
- (c)  $\Delta f/f = 1/450$
- (d)  $\Delta f/f = 1/600$

Note increase in surface uniformity with decreasing  $\Delta f/f$ .



Figure 4: Surface topography of E-B glazed samples. (a), (b) and (c) are higher magnification surface micrographs of Figs. 3(b), (c) and (d) respectively.

magnifications such metallagraphic features as martensitic relief effects, slip lines, and a fine solidification cellular structure become evident, see Fig. 5, which is of the same surface as seen in Figs. 3d, and 4c.

The overlapping of glazed zones is clearly seen in cross-sectional view, see Fig. 6. It would seem reasonable that the rather dramatic increase in surface uniformity achieved by repetitive melting and solidification arises from the dispersion or evaporation of surface contaminants. This cleansing promotes progressively better melting of the solid surface by molten liquid during each successive cycle. By examination of the micrographs it is evident that it is possible to eliminate the "ripple structure" and obtain a surface with minimal periodic topographical variation, see Fig. 6. The surface relief effects already mentioned (i.e. martensite platelets and slip lines) are presumably formed by thermal stresses during cooling.

The present experimental results are of interest both from a fundamental and practical viewpoint. For instance, the surface physics involved in producing a smooth surface is of obvious interest and worthy of detailed study. Also, the ability to readily produce high quality surface layers now greatly facilitates the characterization of corrosion, erosion, and wear of rapidly quenched alloys. In conclusion, it should be noted that the highest quality surfaces thus far produced have only a peak-to-trough differential of  $\sim 5\mu$ . This is important in the preparation of rapidly solidified surface layers with an engineering quality surface finish.

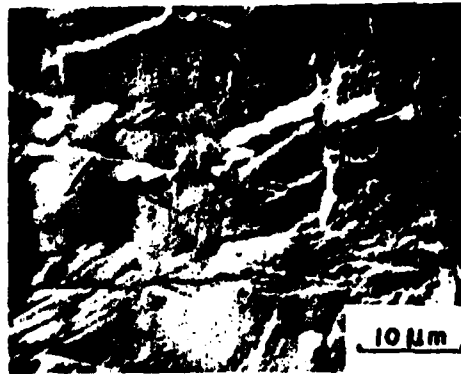


Figure 5: Surface structure of E-B glazed M-2(see also Figs. 3(d) and 4(c)). Note surface relief arising from martensite transformation and slip lines. The fine cellular solidification structure is evident in the background.

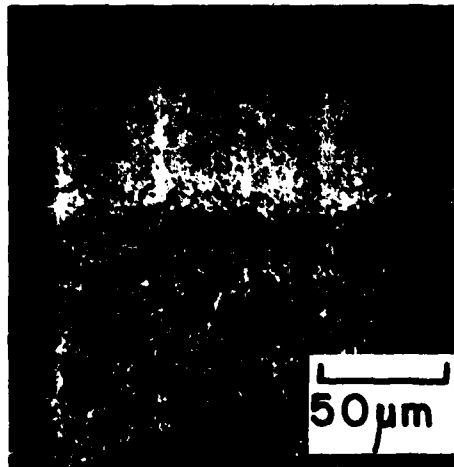


Figure 6: Transverse section of E-B glazed surface showing overlapping zones.

References

1. E. M. Breinan, B. H. Kear, C. M. Banas and L. E. Greenwald: Superalloys: Metallurgy and Manufacture, p. 435, 3rd International Symposium, Seven Springs, PA 1975.
2. P. R. Strutt, H. Nowotny, M. Tuli and B. H. Kear: Mat. Sci. and Engr., 36, (1978), 217.
3. Young-Won Kim, P. R. Strutt and H. Nowotny: Met. Trans. 10A, (1979), 881.
4. S. M. Copley, D. Beck, O. Esquivel, and M. Bass: Laser-Solid Interactions and Laser Processing: p. 161, Amer. Inst. of Physics, Conference Proceedings, Number 50, 1979.
5. R. Mehrabian, S. Kou, S. C. Hsu, A. Munitz: Laser-Solid Interaction and Laser Processing: p. 129, Amer. Inst. of Physics, Conference Proceedings, Number 50, 1979.
6. W. M. Steen: Conference on Rapid Solidification Proceeding, Reston, Virginia 1980.
7. W. Gruhl, B. Grzemba, G. Ibe, and W. Hiller: "Aluminum", 53, (1977), 177.
8. T. R. Tucker, J. D. Ayers and R. J. Schaefer: Laser and Electron Beam Proceeding of Materials: p. 760, Academic Press, 1980.
9. B. G. Lewis, P. R. Strutt: Conference on Rapid Solidification Proceedings, Reston, Virginia, 1980.
10. R. Mayer, W. Dietrich, and D. Sundermeyer: Welding Journal, June 1977.

SECTION II

The following three papers were presented at conferences in the period Fall 1979 - Spring 1980: respectively -

- (i) Materials Research Society Annual Meeting  
November 26th - 30th 1979. Cambridge, MA.
- (ii) Spring Meeting of TMS-AIME  
February 1980, Las Vegas (in press).
- (iii) 2nd International Conference on Rapid Solidification Processing  
March 1980, Reston, VA. (in press).

(i) Laser and Electron-Beam Melting of  
Iron-Base Hard Materials

B. G. Lewis, D. A. Gilbert and P. R. Strutt

Department of Metallurgy  
University of Connecticut  
Storrs, Connecticut 06268

Hardness values above those obtained by conventional heat treatment have been found in the rapidly solidified melt zones of electron beam and laser surface melted iron-base hard materials.

In this study a range of alloys have been examined, M2 tool steel, Fe-TiC pseudo-binary eutectic system and a selection of cemented carbides with both martensitic and age hardening matrices. Preliminary hardness data and microstructural observations are presented and the improvements in hardness obtainable in rapidly quenched glazed zones are discussed in terms of grain refinement, greater solid solution hardening and subsequent ultra fine precipitation on tempering/aging.

## 1. Introduction

The major strengthening mechanisms in alloy steels are grain size refinement, solid solution strengthening and dispersion (and precipitation) hardening. The various levels of strength and toughness can be discussed in terms of these, or combinations of these mechanisms (1).

The Hall-Petch equation, which relates yield strength ( $\sigma_y$ ) to grain size ( $\lambda$ ) by

$$\sigma_y = \sigma_i + k\lambda^{-1/2} \quad (1)$$

where  $\sigma_i$  refers to the stress needed to move dislocations in a grain and  $k$  is a constant, points to the advantages of a fine grain size. Toughness is also sensitive to grain size and refinement of grain size can lead to improved toughness by way of a reduced impact transition temperature.

Suitable alloying elements bring about strengthening in steel by solid solution hardening. The degree of hardening increases with solute content towards the solubility limit.

The strengthening produced by dispersion hardening (or precipitation hardening in the case of maraging steels) can be described by an Orowan model such that the yield stress of the steel is given approximately by

$$\sigma_y = \sigma_m + \frac{\alpha \mu b}{L} \quad (2)$$

where  $\sigma_m$  is the yield stress of the matrix (and can include contributions from all other hardening mechanisms),  $\alpha$  is a constant,  $\mu$  is the stress,  $b$  is the Burger's vector and  $L$  is the mean particle spacing. According to the above equation high strength alloys are favored by ultra fine dispersions of particles/precipitates.

Recent research in the field of rapid quenching has shown possible significant improvements in the areas outlined above: refinement of as-cast grain size to sub-micron levels, extensions of solid solubility limits and associated modifications of precipitation behavior.

Several studies of the effect of rapid quenching on iron-base materials have been made (2-7) and these indicate improvements in strength levels (hardness) that increase with quench rate.

## 2. Materials and Techniques

Samples of M2 tool steel and arc melted buttons of Fe-37 Vol%TiC were scanned by a 3kW continuous CO<sub>2</sub> laser with a 0.5 mm beam size. Thin melting passes were made over the M2 steel at velocities in the range 12.5-75 cms.sec.<sup>-1</sup> corresponding to melt depths of 250-25  $\mu$ m, respectively. A slow homogenizing pass was first made on the Fe-TiC alloy in order to dissolve the particularly large carbides present in the as-cast buttons. This treatment was followed by a thin pass at 50 cms.sec.<sup>-1</sup> which generated a melt zone  $\approx$ 130 $\mu$ m deep.

Samples of cemented carbide from Chromalloy Sintercast Div. (West Nyack, N.Y.) were glazed in vacuum by a low power electron beam. The power requirements for electron-beam glazing are considerably less than for a laser because of the highly efficient beam-substrate coupling (8). Under similar glazing condition an order of magnitude less beam power is necessary to achieve equivalent melt depths. A single slow (4.25 cms. sec.<sup>-1</sup>) pass was made over the cemented carbides at a power of 375 watts and this gave a melt depth of  $\approx$ 450  $\mu$ m. No cracking was observed at this glazing speed.

The alloys used in this study and the melting conditions used are summarized in Table I.

Following glazing, samples were sectioned for metallographic examination. Knoop (500 gm) hardness measurements were made through the zones in the as-glazed and the tempered (or aged) condition. The hardness of the standard condition of the alloys was also determined.

Table I. Alloy Compositions and Surface Melting Conditions

Alloy (Approx.wt.%)	Beam Power (kW)/ Scan Rate (cms.s <sup>-1</sup> )	Melt Depth ( $\mu$ m)	Cooling Rate (deg.C.s <sup>-1</sup> )
M2 Cr 4 V 1.5 Mo 5 Co 6 W 6 Bal.Fe	3/12.5 (Laser)	250	$\approx 10^5$
FeTiC 37Vol%TiC Bal.Fe	3/50 (Laser)	130	$4 \times 10^5$
<u>Cemented Carbides</u>			
SK 36Vol%TiC Cr 5 Co 4 Mo 4 Bal.Fe Ni 0.5			
MS 5 41Vol%TiC 14 Cr+NiMoCoTi Bal.Fe	0.375/4.25 (Electron Beam)	450	$10^4 - 10^5$
M 6 45Vol%TiC 18 Ni+MoCoTi Bal.Fe			

### 3. Results

#### A. M2 Tool Steel (3)

The standard hardness for M2 in the quenched and tempered condition is about 750 KHN. Following glazing, a hardness of  $\approx 1000$  KHN is observed, characteristic of untempered martensite. The martensitic structure is unresolved (Fig. 1), the main features of the glazed microstructure being a cellular eutectic like structure bounded by a carbide network.

X-ray and magnetic measurements on segments spark machined from the zone, together with the etching characteristics, indicate the existence of martensite plus 20% austenite in the quenched zone. On tempering (two periods of 1-1/2 hours at 560°C) the hardness falls to 850 KHN which is 10-15% higher than conventionally treated M2.

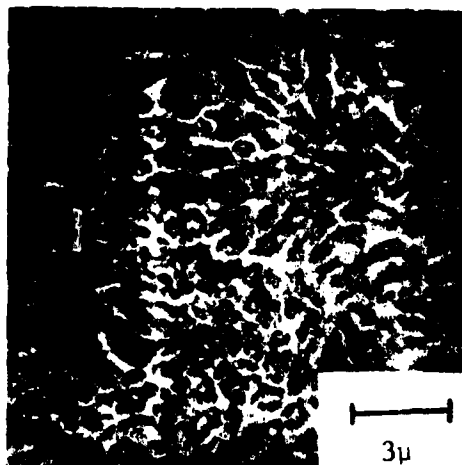


Fig. 1 SEM micrograph of M2 tool steel glazed and tempered (etched in Vilellas reagent).



Fig. 2 SEM micrographs of glazed Fe-37vol%TiC (etched in Vilellas Reagent).

B. Fe-37Vol%TiC (9)

The as-received hardness of this pseudo-binary hypereutectic alloy is  $\approx 550$  KHN. Laser glazing raises this substantially to values in the range 1100-1300 KHN. The microstructure of the glazed zone is depicted in Fig. 2.

The zone is characterized by TiC dendrites embedded in a matrix of equiaxed cellular structure similar to that seen in M2. The nature of the carbide network in this case must be different since no alloying elements are present and the solubility of Ti/TiC in Fe is limited ( $\leq 0.5\text{wt\%}$ ) (10,11). The high hardness values would indicate a martensitic matrix although no lath morphology is observed. The quench rate ( $\geq 10^5 \text{ deg.C.s.}^{-1}$ ) is sufficient for a martensitic transformation in nominally pure iron (6) although powder x-ray diffraction did not reveal any tetragonality. Tempering (cf M2 treatment) reduced the hardness to between 600-700 KHN. This reduction, to close to the as-received value, is not unexpected in view of the absence of any secondary hardening alloying elements.

### C. Cemented Carbides

#### (i) Alloy SK (Tool Steel Matrix)

The behavior of SK is similar to that of M2 tool steel. An as-glazed untempered martensite is formed containing (as for Fe-TiC) dendritic carbides in an unresolved matrix (Fig. 3). This structure softens on tempering to a value which is higher than that obtained by standard heat treatments. The hardness results are shown in Fig. 4 where it can be seen that glazing brings about approximately 12% increase in final hardness (846 KHN + 949 KHN).

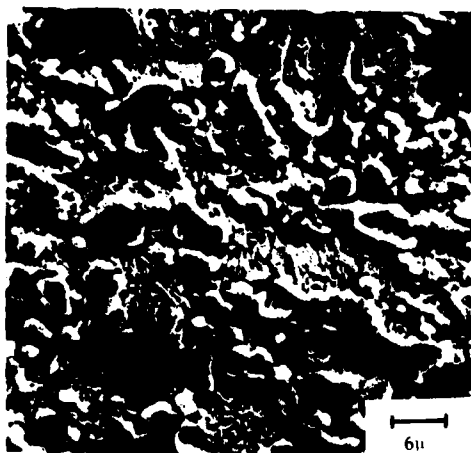


Fig. 3 Alloy SK glazed and tempered. SEM micrograph. Electrolytic etch, 6V, 30 secs. in  $(\text{NH}_4)_2\text{S}_2\text{O}_8$  Soln. (2 gm. in 100 ml  $\text{H}_2\text{O}$ ).

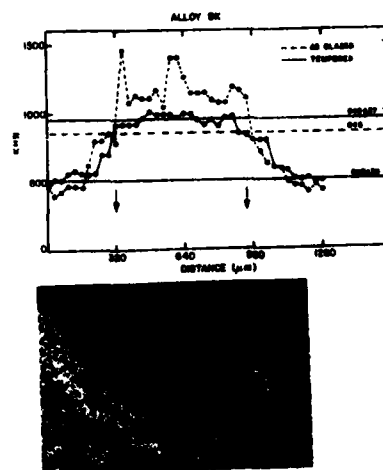


Fig. 4 Hardness data for alloy SK

#### (ii) Alloys MS-5 and M6 (Maraging Steel Matrix)

In the as-glazed condition the maraging matrix cemented carbides are slightly harder than in the annealed condition - perhaps indicative of increased solid solution hardening on rapid quenching. These alloys are microstructurally similar to the ferrotic alloy and to SK (Fig. 5).

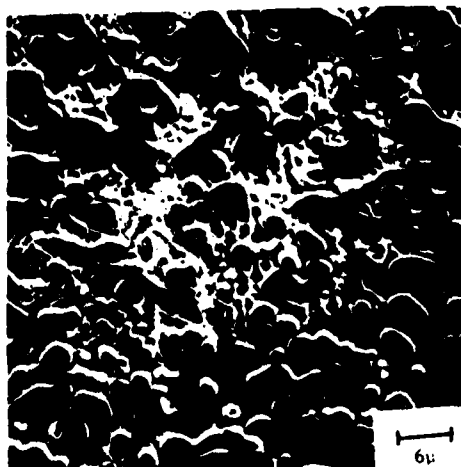


Fig. 5 Alloy M6 glazed and aged. SEM micrograph, electrolytic etch.

There is a network of TiC dendrites together with undissolved carbides in an unresolved matrix. On heat treatment the zones in both MS-5 and M6 age to a higher hardness than the rest of the sample. The results of through zone hardness for MS-5 and M6 are given in Figures 6 and 7.

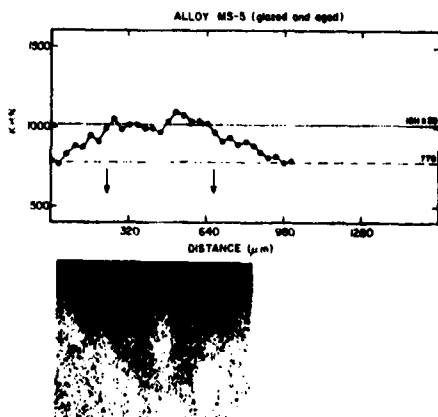


Fig. 6 Hardness data for MS-5

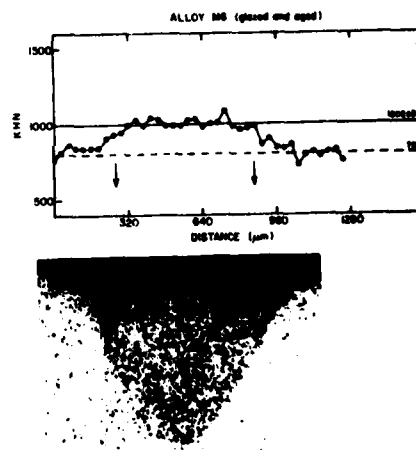


Fig. 7 Hardness data for M6.

MS-5 shows an increased hardness of about 30% (776 KHN-1011 KHN) and M6 about 25% (799 KHN-1002 KHN).

#### 4. Discussion

The increase in hardness of M2 tool steel following glazing and tempering arises from microstructural refinement and, due to the greater retention of alloying elements in solution at the high cooling rates, possibly a finer dispersion of carbides appearing on tempering.

In the case of the Fe-37Vol%TiC two effects were expected, microstructural refinement and carbide refinement. The hardness of the alloy should scale with  $\lambda^{-1/2}$ , (where  $\lambda$  can be taken to refer to either scale of microstructure or carbide size. See Eq. 1). However, following tempering there is only a small increase in hardness over the as-cast condition indicating that carbide refinement, which is unaffected at the tempering temperature, is only second order in its effect on alloy hardness (at least at these ( $\approx 40$ ) Vol.% carbide). The presence of fine scale martensite in the as-glazed alloy is remarkable in its effect, however, increasing the hardness level to  $\approx 1150$  KHN.

For a similar alloy containing secondary hardening elements - alloy SK - the glazing followed by tempering does improve the hardness. That the effect is no more pronounced than for M2 tool steel again shows that carbide refinement is not a major influence on hardness.

The significantly increased zone hardnesses found on age hardening alloys MS-5 and M6 undoubtedly arise from the increase in the amount of solute held in solution at the cooling rates imposed. This, together with the high point defect concentration expected at high cooling rates, can reduce the inter-precipitate distance ( $L$ , Eq. 2) thus increasing the hardness.

#### 5. Acknowledgements

This work is supported by the Office of Naval Research under Contract N00014-78-C-0508.

#### 6. References

1. R.W.K. Honeycombe, Structure and Strengths of Alloy Steels, Climax Molybdenum Co. Ltd., (London).
2. J.J. Rayment and B. Cantor, Rapidly Quenched Metals III, 1, p. 85, Ed. B. Cantor, The Metals Society, London (1978).

3. Y. Kim, P. R. Strutt and H. Nowotny, Metall. Trans. A, 10A, 881 (1979).
4. J.V. Wood, J.K. Bringham and J.V. Bee, Rapidly Quenched Metals III, 1, p. 95. Ed. B. Cantor, The Metals Society, London (1979).
5. Y. Inokuti and B. Cantor, J. Mat. Sci., 12, 946 (1977).
6. F. Duflos and B. Cantor, Rapidly Quenched Metals III, 1, p. 110. Ed. B. Cantor, The Metals Society, London (1978).
7. E. M. Breinan, B. H. Kear, C. M. Banas and L. E. Greenwald, in Superalloys: Metallurgy and Manufacture. Ed. B. H. Kear, Claitors Publ. Div., Baton Rouge, LA (Sept. 1976), p. 435.
8. P. R. Strutt, Mater. Sci. Eng. (1979) (In the press).
9. D. A. Gilbert, M. S. Thesis, Univ. of Connecticut (1979).
10. R. Edwards and T. Raine, Plansee Proc., p. 232 (1952).
11. V. N. Eremenko, Zhur, Meorg. Khimii., 9, 2131 (1956).

(ii) Microstructure Control by  
Electron-Beam Surface Melting Techniques

B. G. Lewis, D. Gilbert, P. R. Strutt

Department of Metallurgy  
University of Connecticut  
Storrs, Connecticut 06268

## 1. Introduction and Background

Over the last decade research into rapid quenching from the melt has presented the metallurgist with many novel materials and structures. There are numerous effects which rapid quenching has on the as quenched structures, and these in turn influence the reactions during subsequent heat treatment. The more important modifications associated with quench rate are extensions of solid solubility, refinement of microstructure and modification of segregation patterns and the formation of metastable phases.

By its very nature rapid quenching does not immediately lend itself to practical applications and it is only the recent use of directed energy sources (1), employing self substrate quenching, that has opened up the possibility of profitable surface melting treatments.

The present authors have shown that both laser (2) and electron beam glazing (3) of M2 tool steel can give a degree of homogenization and microstructural refinement unattainable by conventional heat treatments. The glazing process provides complete dissolution of the carbide phases, including MC, leading to a fine scale solidification structure containing no coarse carbide particles. Significant improvements in hardness are brought about by the scale of the microstructure and also the sub-micron carbide precipitates within the martensite matrix.

In this paper we present a summary of the microstructures found on electron-beam glazing and tempering M2 tool steel, and the results of initial experiments using a novel technique for glazing large surface areas using electromagnetic deflection of the electron-beam. The potential applications of these techniques are briefly discussed.

## 2. Electron-Beam Glazing

Electron-beam technology is much used industrially for both welding and heat treatments. The present application makes use of a low power (<2 kW) Zeiss electron-beam welding unit to melt thin surface layers of tool steel which are then rapidly quenched by virtue of the intimate contact between the molten layer and the substrate. Conventionally, in the process known as laser (1) or electron-beam glazing, the directed energy source is fixed and the workpiece is mechanically scanned through the beam, Fig. 1(a). Scan rates between 1 and 400 cms.sec<sup>-1</sup> have been used with a beam diameter of 0.3 mm and power of 375 watts. At the low speeds melt depths up to 200  $\mu$ m were obtained while at 400 cms.sec<sup>-1</sup> beam penetration was less than 10  $\mu$ m. The corresponding cooling rates vary from  $\sim 10^4$  deg. C.sec<sup>-1</sup> -  $\sim 10^6$  deg. C.sec<sup>-1</sup>. In order to cover significant areas of material complicated apparatus is required to manipulate the sample. A distinct feature of electron-beam glazing, however, is the possibility of rapid scanning of an entire surface by electromagnetically deflecting the beam, Fig. 1(b). In our laboratory a special wave form generator has been designed and constructed for the X-Y beam deflection coils of the Zeiss electron-beam unit. A glazed area is thus produced by applying two nearly equal frequency triangular waves to the deflection coils forcing the beam to trace out a succession of rectangular Lissajous' figures. In this way a given set of quenching conditions can be imposed quickly and evenly over several square centimeters of steel.

## 3. Microstructure and Hardness of Glazed M2 Tool Steel

The microstructures of M2 tool steel, austenitized at 1230°C and oil quenched and also following tempering (120 minutes at 560°C) are shown in Figs. 2(a) and (b). These micrographs are included for comparison with the microstructures shown in Fig. 3(a) and (b) which are typical of an electron beam glazed zone. In the conventionally treated steel coarse (up to 3  $\mu$ m) carbides are present within grains and at grain boundaries. Fig. 2(a) shows

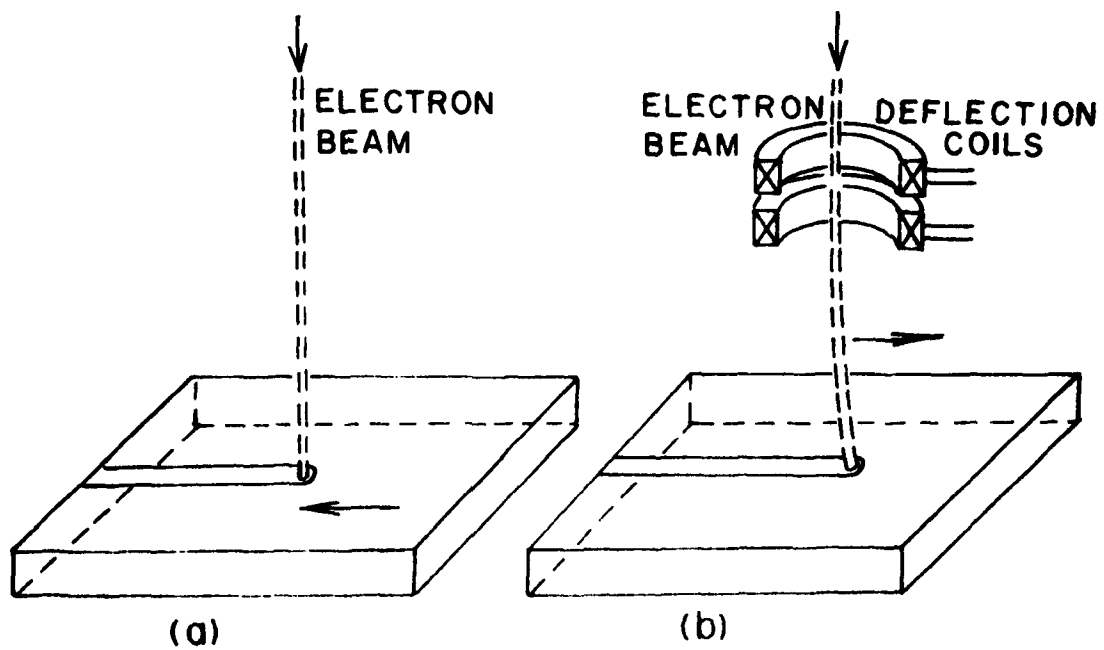


Fig. 1 Schematic diagram of the electron beam glazing process showing (a) fixed beam, moving workpiece, (b) fixed workpiece, scanned beam.

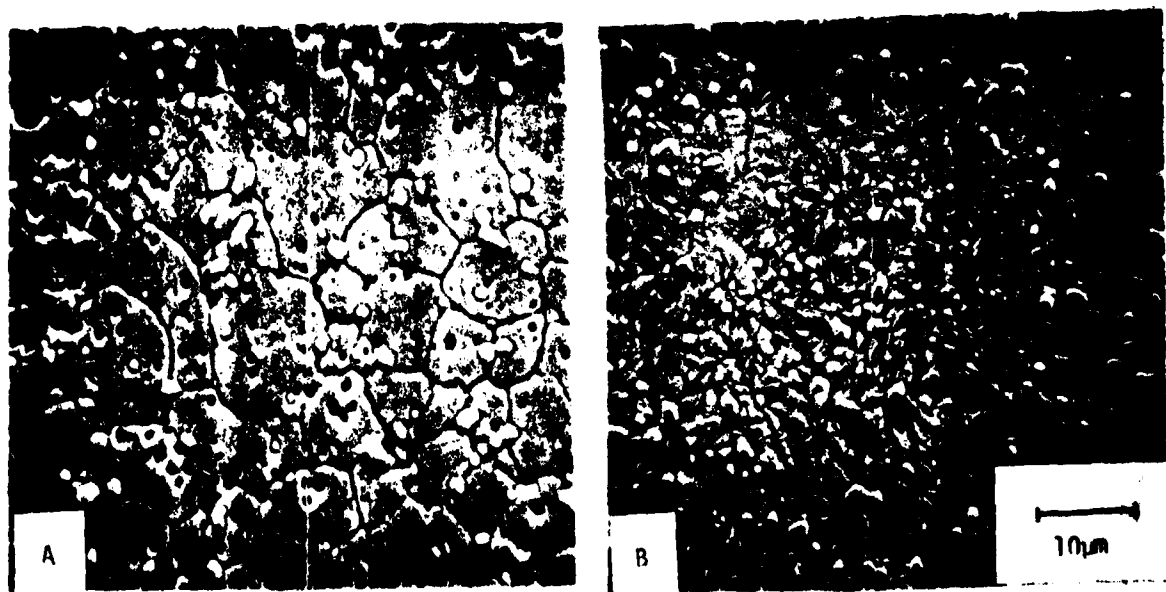


Fig. 2 Scanning electron micrograph of M2 tool steel etched in Vilella's reagent (a) austenitized, 1230°C and oil quenched, (b) as in (a) following a single tempering treatment.

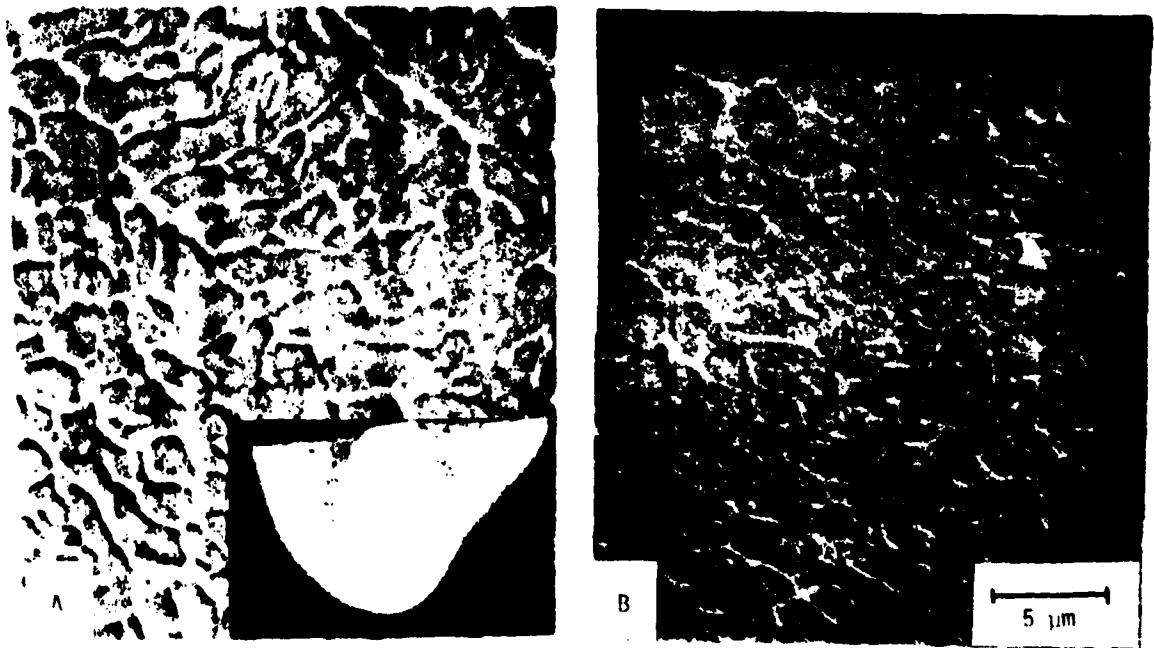


Fig. 3 Scanning electron micrograph of regions of a glazed zone of M2 (a) as glazed, (b) following tempering at 560°C for 120 minutes. Etched in Vilella's reagent.

untempered martensite in the as quenched state. After tempering, etching reveals the martensite laths Fig. 2(b). The grain size depends critically on the austenitizing treatment and in this case a mean grain size of  $\sim 10 \mu\text{m}$  is seen.

Following glazing the carbides, clearly in evidence in Fig. 2, have been almost fully solutionized and the fine solidification structure is characterized by regions of untempered martensite surrounded by a continuous network of carbide in the form of a cellular eutectic. The scale of this microstructure is  $\sim 2 \mu\text{m}$  with some elongation of the cells in the direction of heat flow. The structure is very resistant to etching but following tempering a background structure of tempered martensite is resolvable, Fig. 3(b).

In detail the microstructure of glazed M2 varies with the depth of the zone. Fig. 4 shows a cross section of a glazed zone of M2. The external surface is to the top of the micrograph and the maximum melt depth corresponds to the lower interface of the relatively structureless region, Fig. 5(c). The heat affected zone is below this interface and the grain boundaries and undissolved carbides of the parent steel are clearly evident. Fig. 5(a), (b) and (c) are higher magnification scanning electron micrographs of Fig. 4. The dark etching phase, with increasing predominance towards the surface, is either retained ( $\delta$ ) ferrite or heat affected (tempered) martensite. The lightly etched phase is mainly untempered martensite. An important feature of the microstructure is the typical peritectic reaction, Fig. 5(a), formed as  $L + \delta \rightarrow \gamma + \text{carbides}$ .

Associated with these microstructures are very high hardnesses. The hardness varies down the zone from  $\sim 800 \text{ VHN}$  ( $64 R_C$ ) at the top surface to  $\sim 1000 \text{ VHN}$  ( $69 R_C$ ) near the melt parent interface. Many aging treatments have been applied to the glazed zones and it was found that a simple aging treatment (3 periods of 120 minutes  $560^\circ\text{C}$ ) increases the hardness levels of



Fig. 4 Variation of microstructure through zone of glazed M2.



Fig. 5 High magnification micrographs corresponding to regions (a), (b) and (c) in Fig. 4.

the zone by about 10%. The optimum and highest uniform zone hardness, however, was obtained by a post glazing heat treatment involving a brief austenitizing (1230°C), liquid nitrogen quench and triple temper. In this way a hardness of between 900-1020 VHN ( $\sim 68 R_C$ ) was obtained to be compared with a value of above 850 VHN ( $\sim 66 R_C$ ) for conventionally treated M2.

#### 4. Characterization of Electron-Beam Scanned Surfaces

The glazed region on a M2 tool steel substrate shown in Fig. 6(a) was produced by electron beam scanning using X and Y frequencies of 30 and 29.92 hertz respectively. A higher magnification view, together with a cross section of the glazed area is shown in Fig. 6(b). The excellent quality of the surface is clearly evident in both Fig. 6(a) and (b). There is a complete absence of surface ripples, and the height differential from peak to trough of the periodic surface undulations is minimal, in fact the entire field of view is in focus even at high magnifications in the optical microscope. The cross sectional view shows remarkable smoothness at the melt-substrate interface. Studies to date have shown that repeated melting and solidification is necessary to attain any degree of surface smoothness. An important factor in this progressive increase in surface smoothness may be the elimination of contaminants, that is the vaporization and dispersion of surface impurities, thus reducing the surface tension and angle of contact of the liquid/solid interface. This cleaning process would lead to a reduction in the height of the liquid bulge which periodically builds up ahead of the moving beam. It is worth mentioning that the best surfaces produced to date have a peak to trough differential of  $\sim 5 \mu\text{m}$ . The mean surface finish tolerance is thus  $\sim \pm 2.5 \mu\text{m}$ .

#### 5. Applications of Surface Glazing Techniques

A wide range of tool materials have been screened by the electron-beam glazing technique and our results indicate that the glazing process could make a significant contribution in the heat treatment of machine tool cutting



Fig. 6 Electron beam scanned area (a) as glazed surface, (b) high magnification of (a) and cross section showing surface modulation and smooth melt/parent interface.

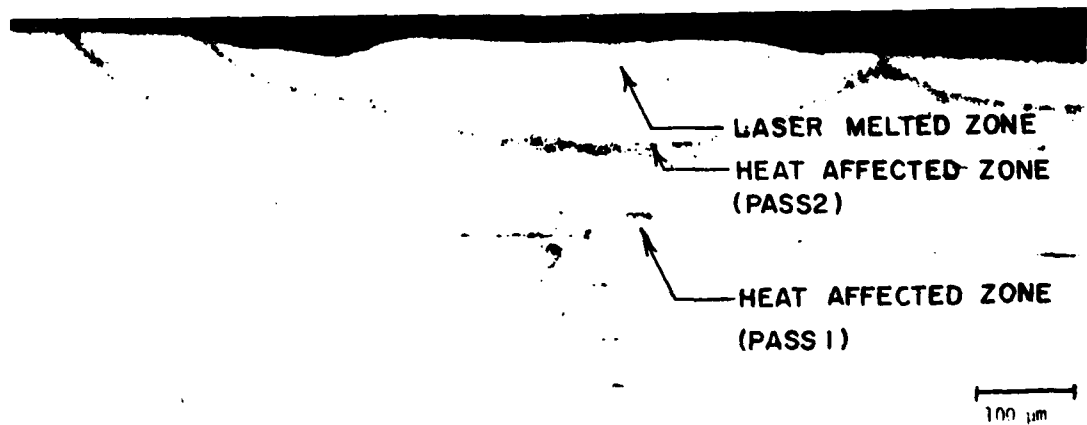


Fig. 7 Melt and heat affected zones of a laser glazed sample of M2 showing the effect of glazing on sulphide inclusions.

edges and bearing surfaces. Further experiments are, however, necessary to determine whether the refined microstructures possess suitable wear and machining properties and tests are, at the moment, underway using area glazed specimens.

A useful property of electron-beam glazed zones that has become apparent from the etching characteristics is their corrosion resistance. Clearly this is an area worthy of further study now that large area glazing is possible.

A more speculative area of application is the use of the area glazing technique for surface chemical refinement. In our experiments we have observed that surface impurities and below surface defects are wiped away by the surface glaze. Fig. 7 shows how sulphide stringers in M2 tool steel are eliminated in the glazed zone and there is even partial dispersion in the heat affected zones. Such treatments may find application in cleaning, for example, the inner surface of ball races in gas turbine engines where subsurface inclusions are a major problem. With surface temperatures approaching the vaporization temperature of iron, it is clear that a degree of "refining" may be possible at the surface of many materials.

#### 6. Acknowledgements

This research is supported by the Office of Naval Research under Contract N00014-79-C0580.

#### 7. References

1. E. M. Breinan, B. H. Kear, C. M. Banas and L. E. Greenwald, "Superalloys; Metallurgy and Manufacture", 3rd Int. Symposium, Seven Springs, PA, pg. 435, 1975.
2. Young Won Kim, P. R. Strutt and H. Nowotny, Met. Trans. A., 10A, p. 881 (1979).
3. P. R. Strutt, D. Gilbert, and M. Kurup, TMS Paper Selection F79-6 (1979).

(iii) Electron Beam Glazed Surface Areas

B. G. Lewis, D. A. Gilbert, P. R. Strutt

Department of Metallurgy  
University of Connecticut  
Storrs, Connecticut 06268

ABSTRACT

An electromagnetic deflection system has been used to produce large areas of electron-beam glazed tool material. A high quality surface finish is obtained and preliminary data show that the effect of overlapping zones need not be detrimental in its effect on hardness. It is possible to glaze large areas of cemented carbides without cracking and such treatments may significantly increase wear life.

## 1. INTRODUCTION

The benefits of ultra-rapid quenching techniques to the metallurgist have been discussed and explored in ever more detail over the last decade; however, with few exceptions, the transfer of rapid quenching technology into the market place has been slow. The development of laser glazing (1) and other directed-energy, self substrate quenching techniques has more recently initiated considerable research into surface treatments with direct industrial applications.

In general laser or electron-beam glazing of a surface is brought about by mechanical movement of the substrate relative to the beam. This produces a single melted pass. Larger areas can be glazed by further movement of the specimen to create overlapping zones or by scanning the surface by careful deflection of the beam. In the case of laser glazing such beam control requires programmed mirror oscillations. A distinctive feature of electron glazing is, however, the possibility of rapidly scanning large surface areas by electromagnetically deflecting the beam (2,3,4) and this paper describes the results of the application of this technique to M2 tool steel and "Ferrotic" cemented carbides.

## 2. TECHNIQUES

Samples of M2 tool steel and a "Ferrotic" 40 vol % TiC in a maraging steel matrix were scanned with a 375 watt electron-beam. Beam movement was controlled by applying two nearly equal frequency triangular waveform signals to the deflection coils. The beam then traces out a succession of rectangular "Lissajous' Figures".

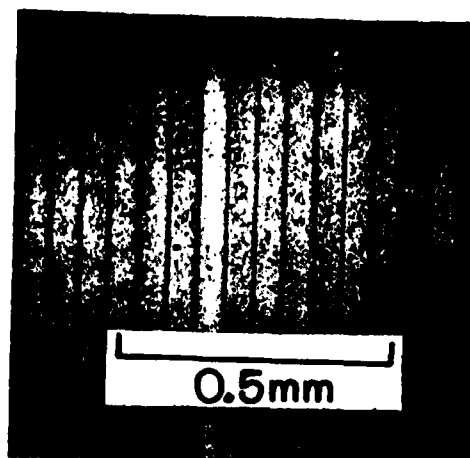
The surfaces were examined by optical microscopy in the as received condition and following sectioning and suitable heat treatment (tempering).



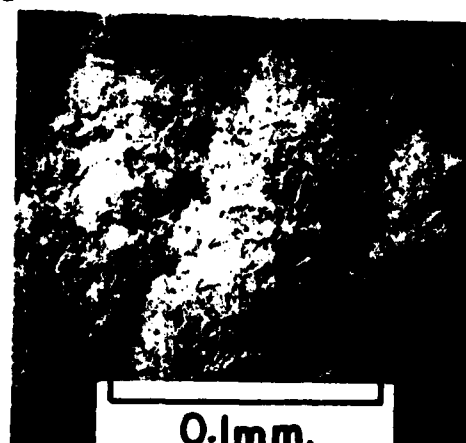
Fig. 1 Top view of surface glazed M2 tool steel.

### 3. RESULTS AND DISCUSSION

An as glazed surface is shown in Figure 1. The frequencies used were 60 and 59.95 hertz. The excellent quality of the surface is evident in Fig. 2. There is a complete absence of surface ripples and the only surface relief features (Fig. 2b) are slip lines, surface martensite and the periodic undulations due to over lapping passes. The best surfaces to date have a peak to trough differential of  $\approx 5\mu\text{m}$ . The quality of finish is also highlighted in Fig. 3 where the over lapping zones are shown in cross section. The melt depth is approximately constant and the microstructure is almost featureless (untempered martensite). The overlap is revealed by the tempering effects in the heat affect zone. The microhardness (50 gm load) of the zone in the as glazed state is  $\approx 770$  DPH, while the heat affect region is somewhat lower at  $\approx 530$  DPH. Following tempering the zone hardness increases to 920 DPH and the heat affected zone becomes less obvious with a hardness 850 DPH. The tempered martensite of the double tempered tool steel ( $2 \times 560\text{C}$  for 2 hours) is shown in Fig. 4. In the background the directionality associated with the solidification structure is visible.



(a)



(b)

Fig. 2. Detailed structure of surface glazed M2.



Fig. 3. Cross section of sample shown in Fig. 2

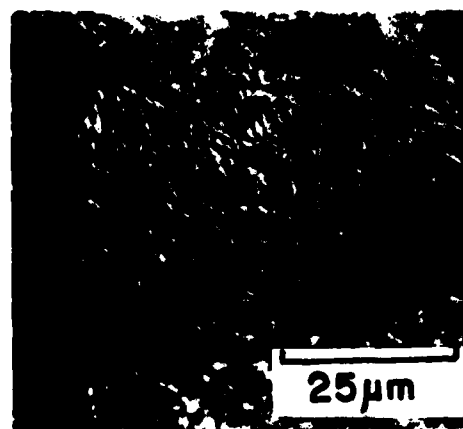


Fig. 4. Tempered structure of surface glazed sample.

Previous work (5) has shown that significant carbide refinement can be achieved on glazing hyper-eutectic TiC tool steel "Ferrotic" alloys and Fig. 5, which shows the top view of a surface glazed sample, highlights this point. The coarse ( $10\text{ }\mu\text{m}$ ) carbides present in the as sintered structure (Fig. 5a) solidify as primary TiC dendrites in the rapidly quenched structure with secondary dendrite arm spacings of the order of  $1\text{ }\mu\text{m}$  (Fig. 5b). It should be noted that no cracking has occurred during glazing either at the surface or at the maximum melt depth (Fig. 6).

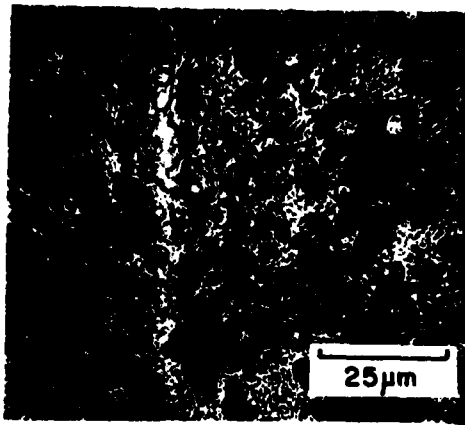


Fig. 5(a). Microstructure of as sintered "Ferrotic" cemented carbide (40 vol.% TiC).

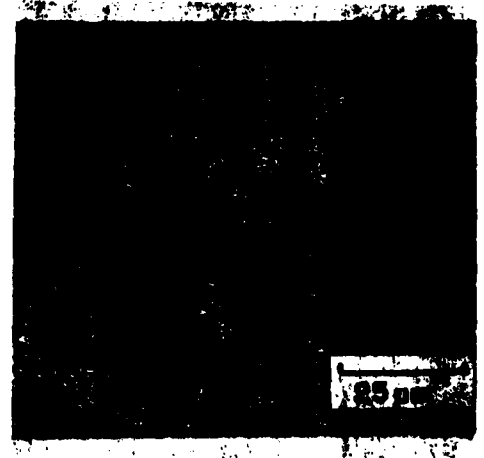


Fig. 5(b). Dendritic TiC surface glazed sample.

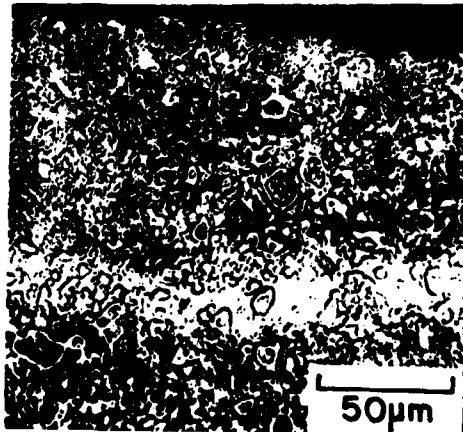


Fig. 6. Cross section of surface glazed cemented carbide.

Since large surface treated areas can now be achieved routinely, this technique can clearly be used to usefully modify and control surface microstructures. Such modifications are likely to improve both wear and corrosion properties as well as increasing basic mechanical properties, e.g., hardness and fracture toughness. Such practical tests are at present underway.

#### 4. ACKNOWLEDGEMENTS

This research is supported by the Office of Naval Research under Contract N00014-78-C0580.

5. REFERENCES

1. E. M. Breinan, B. H. Kear, C. M. Banas and L. E. Greenwald, "Superalloys; Metallurgy and Manufacture", 3rd Int. Symposium, Seven Springs, PA, (1975), pg. 435.
2. B. G. Lewis, D. A. Gilbert and P. R. Strutt, New Developments in the Processing and Properties of High Speed Tool Steels III, Las Vegas, AIME (1980), in press.
3. T. R. Tucker, J. D. Ayers and R. J. Schaefer, Laser and Electron Beam Processing of Materials, MRS, Cambridge, MA, (1979), in press.
4. W. Gruhl, et al., Aluminum, 53, (1977), pg. 177.
5. B. G. Lewis, D. A. Gilbert and P. R. Strutt, Laser and Electron Beam Processing of Materials, MRS, Cambridge, MA, (1979), in press.

SECTION III

## Electron-Beam Glazed Surface Areas - Wear Studies

### 1. Introduction

The electron beam area glazing technique, as applied to tool steels, can be considered an extreme example of case hardening in which the conventional hardening associated with the solid state martensite transformation is modified by the pre-existing refined solidification structure derived from the high liquid → solid cooling rate. (The quality of surface finish obtainable by area glazing, and the consistency of melt depth is illustrated for M2 tool steel in Figures 1, a,b,c.)

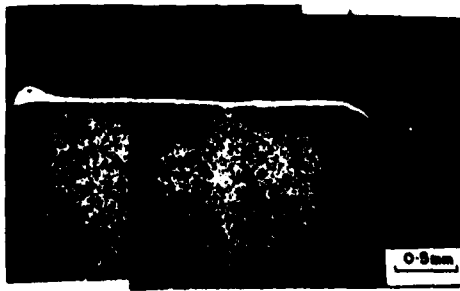
The ability to cover large areas of material has created the possibility of evaluating important macroscopic mechanical properties, and, in this context we have initiated a study of the wear properties of surface treated tool steels. The area-glazing technique, and the structure and hardness of various glazed tool materials are described elsewhere in this report; this section will be confined to a description and discussion of the wear of M2 tool steel and SK (36 vol.% TiC) Ferro-TiC cemented carbide.

### 2. Wear Test Methods<sup>(1)\*</sup>

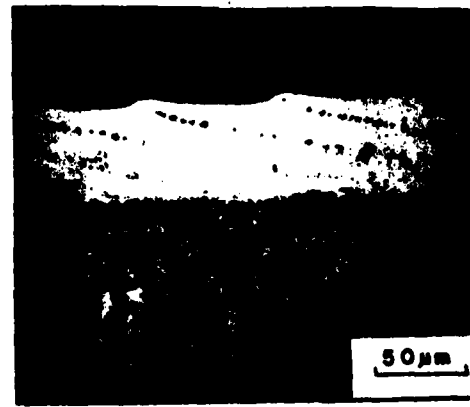
In use, tool steels are usually subjected to a combination of relative motion against both similar and dissimilar materials and the transmission of loads. Materials interactions that involve sliding and impulsive loading, eg. in gears and cams, are described as compound impact (that is, impact under simultaneous sliding) and, in general, lead to the wear of adjacent surfaces.

In view of the difficulties associated with wear testing it is necessary to specify carefully the conditions under which a test is conducted and to keep those conditions fixed when considering the effect of glazing and post-glazing heat treatments on the wear behavior of the tool materials.

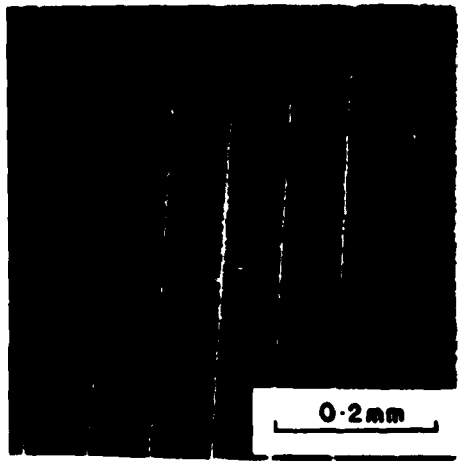
See Acknowledgements, (1) S. L. Rice: Wear 54 (1979), 291-301.



(a)



(b)



(c)

Figure 1:

- (a) Transverse section of electron-beam (E-B) glazed M-2 tool steel.
- (b) Overlapping melt passes of E-B glazed M-2 tool steel.
- (c) Surface morphology corresponding to Fig. 1 (b).

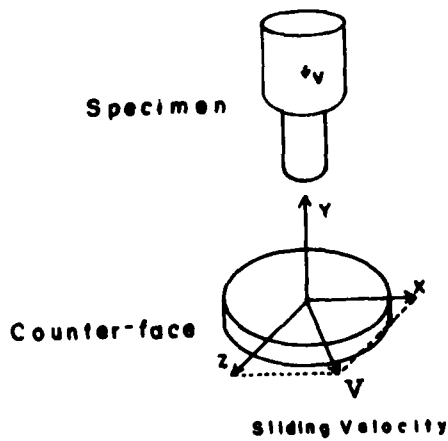


Figure 2: Schematic diagram of wear test geometry.

In the wear test apparatus used in this study<sup>(1)</sup> compound impact wear is simulated by impacting a wear sample with a measured normal impacting force ( $P_N$ ) against a counterface moving with a relative transverse sliding velocity ( $V$ ). A schematic diagram of the wear test and specimen geometry is shown in Figure 2. The controlling external parameters in this arrangement are (a) the relative transverse sliding velocity between the contacting surfaces, (b) the nominal contact stress ( $P_N$ /specimen area, M.Pa.), (c) the number of cycles of the test, i.e., the total frictional contract length, and (d) the counterface material - in this case 17-4 PH martensitic steel.

The tests were performed under dust free atmospheric conditions and evaluation of specimen wear was made using a combination of light microscopy, scanning electron microscopy (SEM) including energy dispersive X-ray (EDX) compositional analysis of the wear surface and sub-surface and sample - counterface pair weight loss measurements.

### 3. Sample Preparation

Samples of M2 tool steel and SK Ferro-TiC were produced in the form of cylinders 5mm  $\phi$  and 40mm long. The ends of the cylinders were area glazed to a depth of about 50  $\mu$ m using the area glazing technique ( $f_0 = 62.5H_3$ ,  $\frac{\Delta f}{f_0} = 1.005$ ). The samples were then cylindrically ground to 3mm  $\phi$  and machined to their final length of 18mm.

Austenitizing and oil quenching and/or double tempering heat treatments either prior to or after glazing were carried out in evacuated quartz tubing.

Samples were mounted in specimen holders using epoxy-resin and abraded in situ on 600 grit SiC paper for 1000 test cycles to achieve an initial average surface roughness ( $R_a$ ) of 0.2  $\mu$ m and to create a specimen surface parallel to the counterface.

#### 4. Results

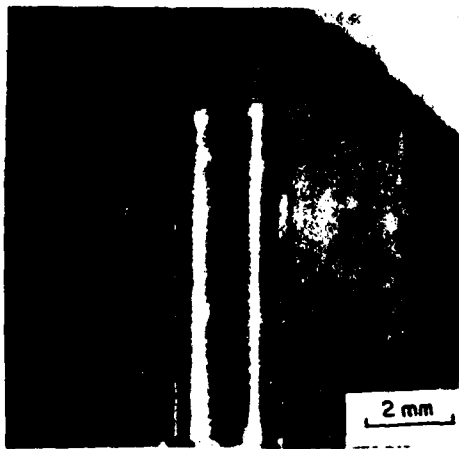
##### (i) M2 Tool Steel

Samples of spherodized M2 tool steel were area-glazed as described in the previous section and examined prior to and following wear testing. No tempering treatment was used in this case.

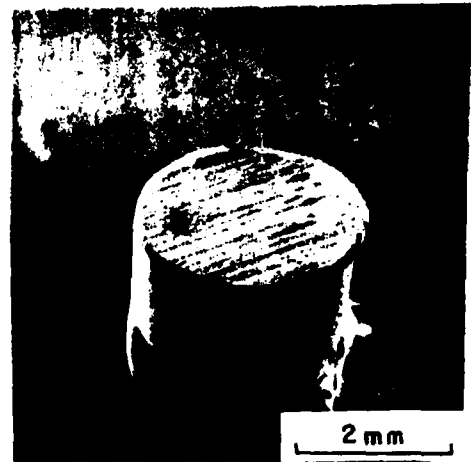
Figure 1 a,b,c shows a transverse section of the as glazed sample. The low magnification micrograph indicates an almost constant melt depth with "end effects" present as either material build-up or edge rounding. (The existence of these glaze-edge effects led us to surface treat the larger diameter samples (5mm  $\phi$ ) and then machine to the final 3mm  $\phi$  standard for the wear test.) The regularity of the overlapping melt zones is depicted in Figure 1b. The interface between melt zones is delineated by a dark etching heat affected (tempered) zone (HAZ) that is softer than the quenched structure. Figure 1c is the surface corresponding to micrograph 1b.

Figure 3a through 3d are low magnification light micrographs of an M2 sample (and counterface) following 5,000 cycles of repetitive compound impact wear with an imposed nominal contact stress of 150 M.Pa. and at a transverse sliding velocity of  $8 \text{ m.s}^{-1}$ . Figures 3a and 3b show evidence of material transport from the counterface to the M2 sample surface and also apparent slip of the glazed layer in the wear direction. The adherence of the 17-4 PH steel to the specimen surface is shown more clearly in Figure 3c around the edges of an unworn glazed region. The wear of the counterface is illustrated in Figure 3d.

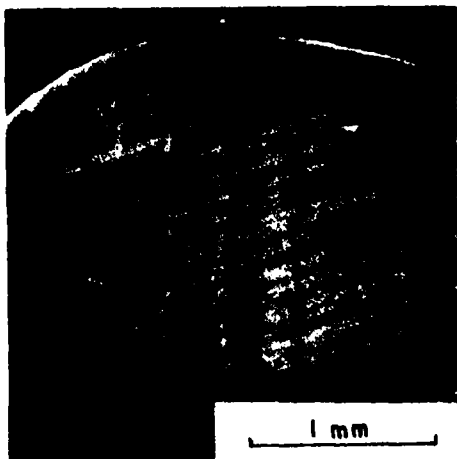
Figure 4a and 4b are montages of the glazed zone before and after wear. The details of Figure 4a have been discussed above and a higher magnification micrograph of a region of Figure 4a is shown in Figure 1b. The important points to note in Figure 4b, the wear micrograph, and the enlarged SEM micrographs, Figures 5 through 9, is the existence of three zones, A, the parent steel, B the glazed



(a)



(b)



(c)

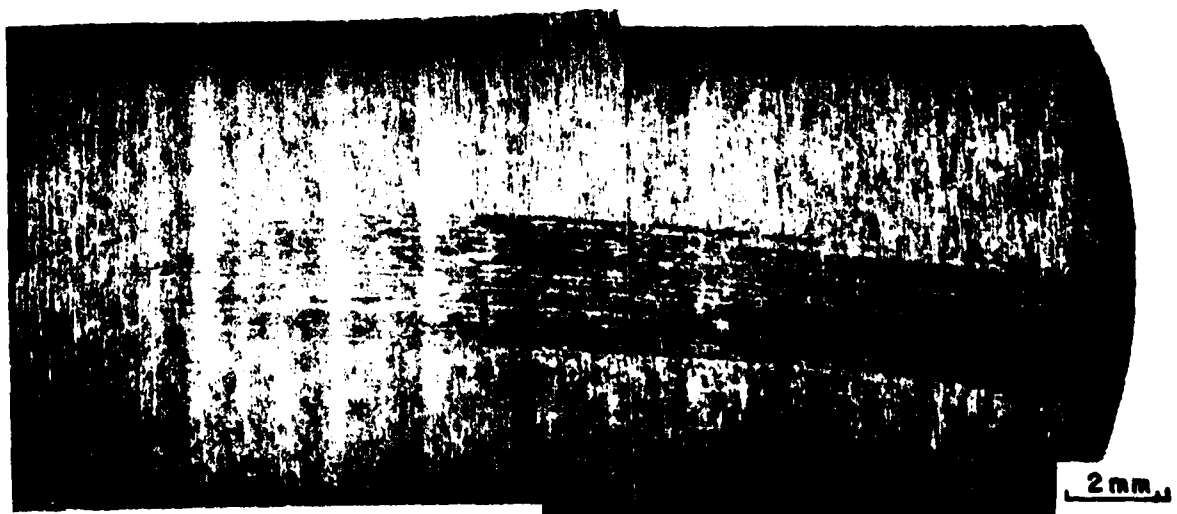
Figure 3: Low magnification micrographs of E-B glazed M-2 following wear test.

(a) Side view of wear specimen

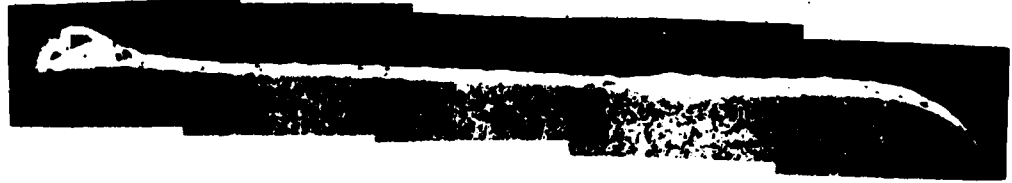
(b) Wear surface

(c) Wear surface, highlighting material transport. Note unworn glazed region at centre left.

(d) Counter-face following wear test.

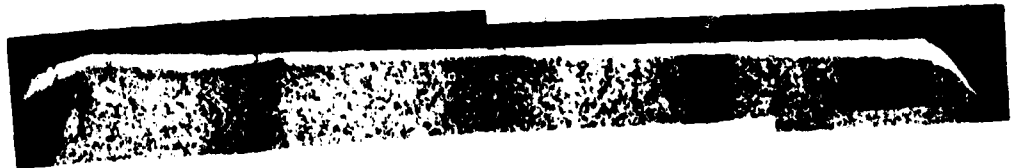


(d)



(a)

Figure 4(a): Cross section of glazed M-2. Note build up of glaze at left hand side and edge rounding at right hand side. (x50)



(b)

Figure 4(b): Post-wear test cross section of glazed M-2. Note removal of glaze build up and the loss of resolution of the overlapping zones. (x50)

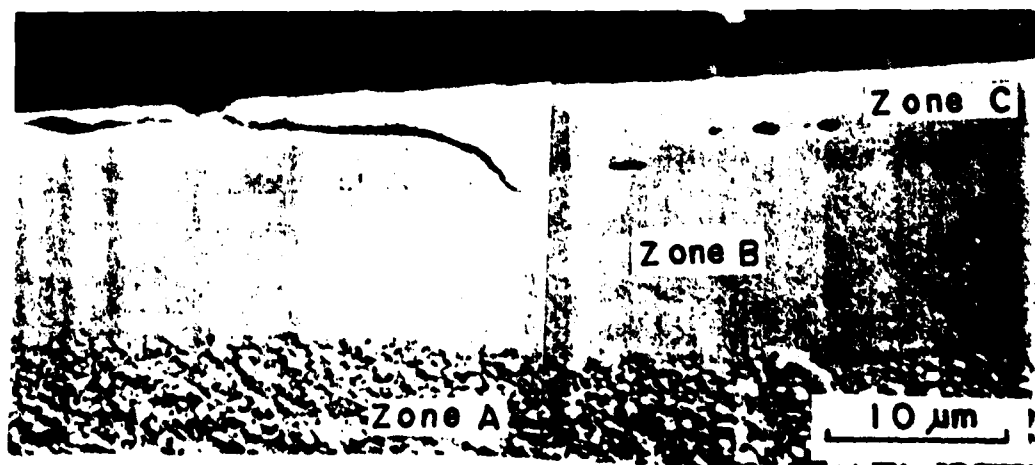


Figure 5: Enlargement of region of Fig. 4(b) showing three zones A, B, and C. and the appearance of cracks and voids in the near surface layer of adhered 17-4 PH counterface material.

zone and C, the near surface zone, and the regularly spaced cracks extending in many cases through all three zones. Following the wear test, no changes are visible in the parent steel, but very clearly the tempered regions between overlapping melt passes, very apparent in the as glazed structure, Figure 1b, have disappeared. The lack of contrast in the glazed zone (untempered martensite is difficult to etch) make it impossible to discuss the possible presence of any plastic deformation during wear, however, the regularly spaced cracks mentioned above are, infact, pulled in the wear direction. The cracks probably arise from the brittle nature of the untempered glazed zones. Nucleation of the cracks appear to occur in the adhered layer/ glazed zone interface (Figures 5 through 9), and terminate in the soft HAZ and spherodized parent M2.

Although macroscopically (Figure 3a) the glazed zone appears to have slipped relative to the bulk sample, there is no evidence for this from the Zone B/Zone A interface, i.e., deformation in the direction of slip. This infers that the slip in Figure 3a arises from the deformation of the glazed build-up depicted in Figure 1a and flow of the transfered zone C material. The crack morphologies of Figures 5 through 9 would support this view.

Studies of the wear of conventionally hardened M2 and glazed and tempered M2 are now being carried out.

(ii) SK Ferro-TiC

Although glazing of Ferro-TiCs can bring about a 10-20% increase in hardness, even after tempering, this may not be the main feature in the wear behavior of cemented carbides. Following glazing there is a significant change in microstructure. Figure 10a shows a typical SK Ferrotic microstructure prior to glazing; present are large angular carbides in a tool steel matrix. Figure 10b is the same steel following glazing; here the carbides are present as primary TiC dendrites in a quenched martensite matrix. This modified microstructure may well lead to improved wear resistance to accompany the established increase in hardness.



Figure 6

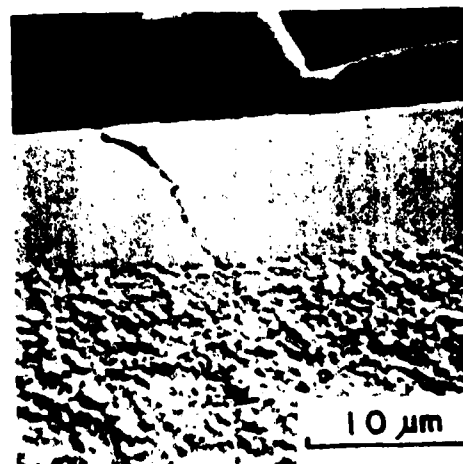


Figure 7

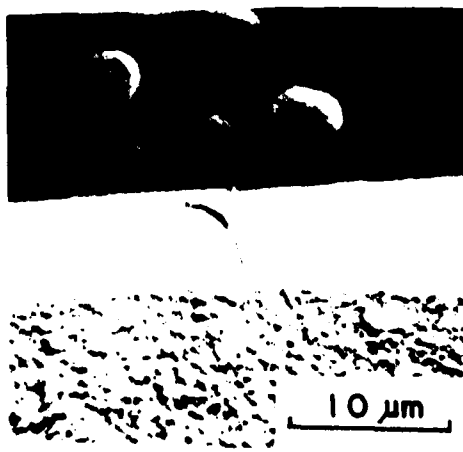


Figure 8

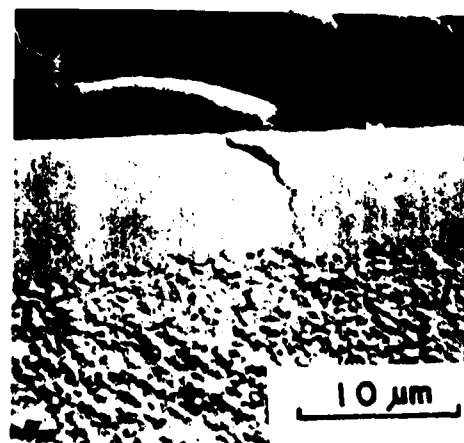
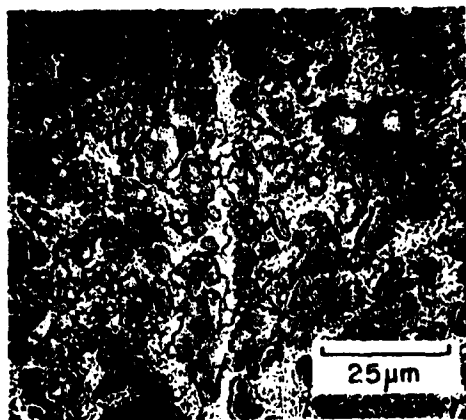
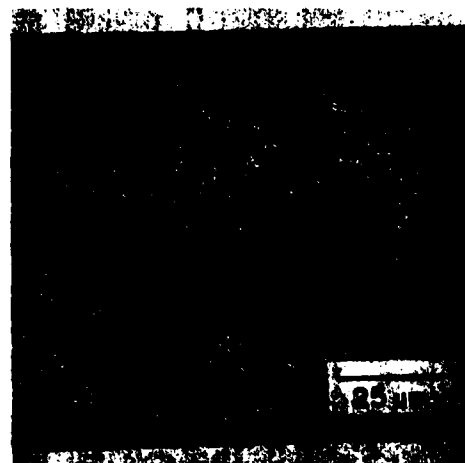


Figure 9

Figures 6-9: Enlarged regions from Fig. 4(b) showing cracks that appear to initiate in Zone C and propagate through to Zone A. Note elongation of cracks in the sliding direction.



(a)



(b)

Figure 10: (a) Microstructure of as sintered SK Ferrotic  
(b) Dendritic TiC in surface glazed SK Ferrotic.

In this initial wear study of Ferro-TiCs the samples were first austenitized and quenched to develop a hardened base material and then glazed but not tempered. This creates a hard (untempered) zone with a softer HAZ as a base. The as glazed sample is shown in Figure 11. The undulations present were removed by the initial in-situ 600 grit abrasion and the sample was subjected to the same test conditions as the M2 steel for 15,000 cycles. There was no significant weight loss during the test, although Figures 12 a,b, and c, which are SEM micrographs of the worn specimen surface, show apparent material transport. Figure 12c reveals evidence of cracking similar to the case for M2. Sectioning of the sample parallel to the sliding direction (normal to the surface cracks, Figure 12c) confirmed (Figure 13a and 13b) the existence of the regularly spaced cracks traversing three distinguishable subsurface zones - Zone A, the coarse carbide parent steel; Zone B, the dendritic carbide zone, glazed to a depth of  $\sim 30 \mu\text{m}$  and Zone C the near-surface layer consisting of adhered 17-4 PH counterface steel (EDX analysis). The subsurface cracks, as in the case of M2 tool steel, appear to initiate in the upper zone and in most instances propagate through the (brittle) glazed zone terminating in the relatively ductile heat affected zone. Figures 14 and 15 show higher magnification SEM micrographs of the cracks. There appears to be no preference for either inter-(dendritic) carbide or trans-carbide fracture, with aspects of both mechanisms present.

As revealed by EDX analysis there is some exchange of material between the counterface and the wear sample. Trace amounts of Ti were detected in the adhered counterface indicating the removal of small amounts of TiC which, as shown in Figure 16 are carried up and laterally in the wear zone. The Ti (TiC) content of the near surface zone increases with approach towards the Zone B/Zone C interface. No judgement could be made concerning the "mixing" of the counter-

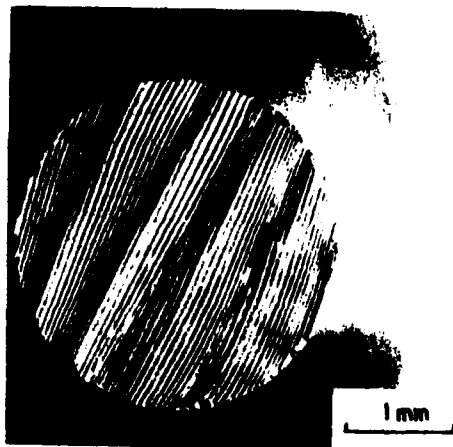
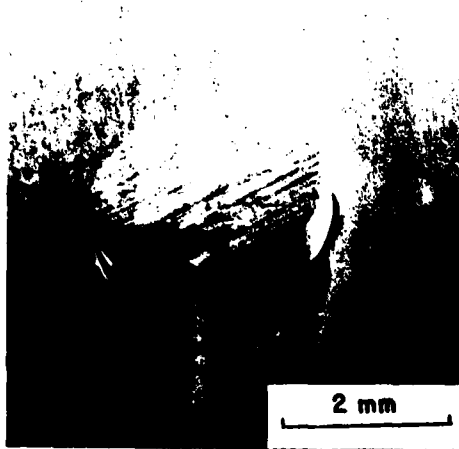
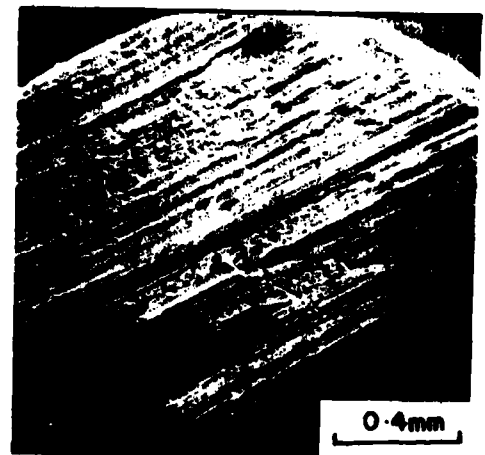


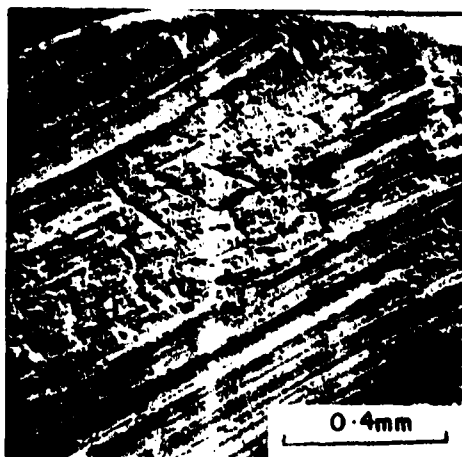
Figure 11: Surface of as glazed SK Ferroitic.



(a)

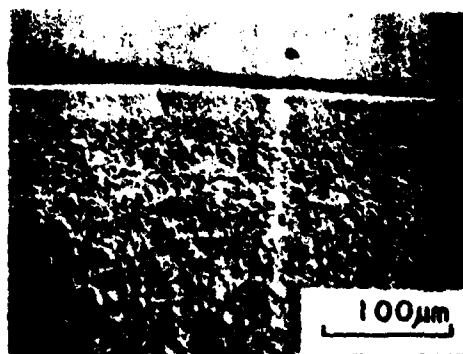


(b)



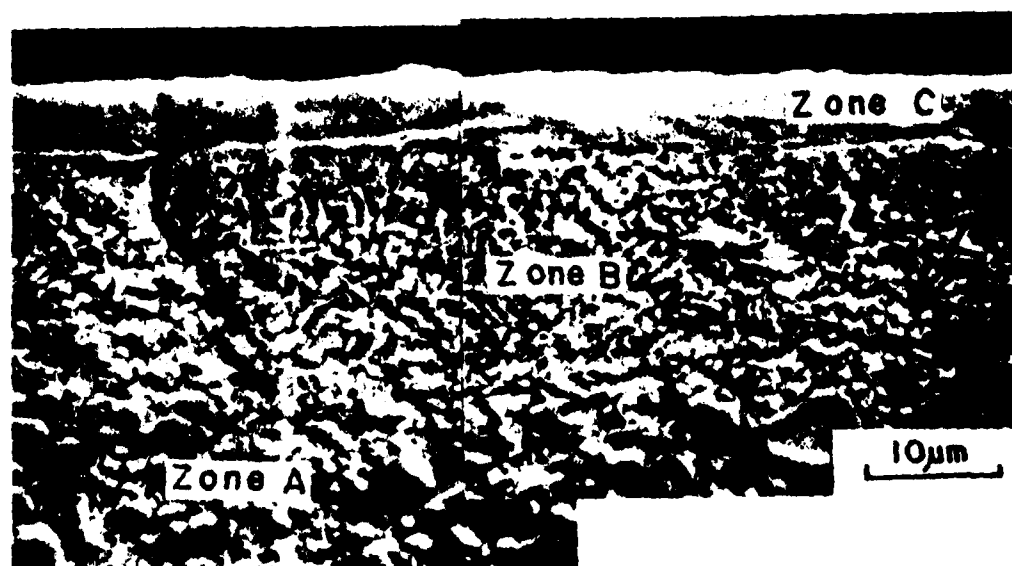
(c)

Figure 12: SEM micrographs of glazed SK following wear test. Note evidence of material transport and surface cracks (Figs. 12b, c).



(a)

Figure 13: SEM micrographs of worn SK sectioned parallel to the sliding direction. Note existence of three zones A, B, and C and also cracking similar to M-2 case.



(b)

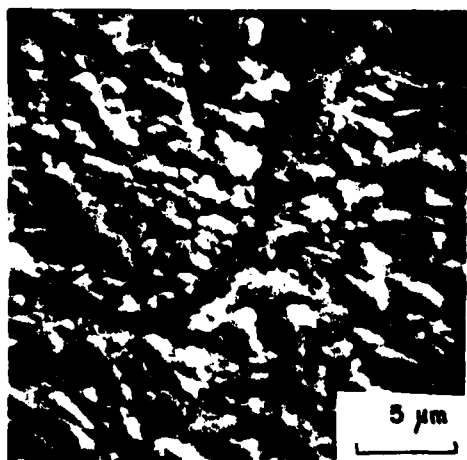


Figure 14

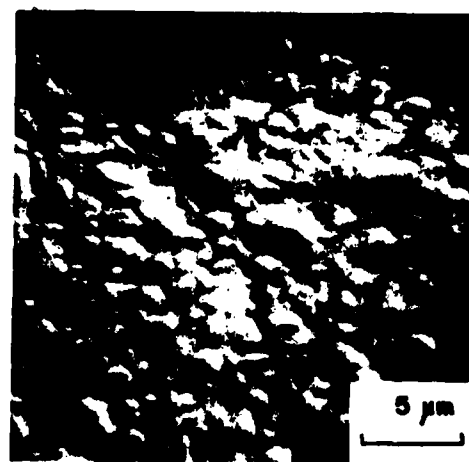


Figure 15

Figure 14&15: SEM micrographs of cracked regions in Fig. 13.

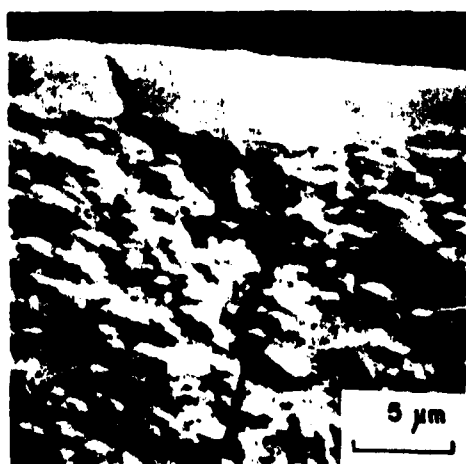


Figure 16: SEM micrograph of worn SK showing existence of carbides in Zone C.

face material into the glazed zone because of the compositional similarity between the 17-4 PH and SK Ferro-TiC steels. There is, however, morphological evidence for mixing, Figures 15 and 16 where it appears that a small amount of the near surface layer has been swept into the top of the cracks through Zone B. In general, the degree of wear at the Zone B/Zone C interface appears minimal, Figure 17, exhibiting no detectable plastic deformation other than in the near surface adhered layer with little carbide removal. The final average surface roughness (Ra) was 1.5-1.75  $\mu\text{m}$ .

To directly compare this wear behavior with that of the standard (coarse carbide) Ferro-TiC the glazed region described above was removed using a diamond wafer blade and the remaining stub, following in-situ preparation was subjected to an identical wear test.

In this case less material transport (adherence) was observed, Figure 18, and transverse sectioning revealed no subsurface cracks, Figure 19. Here three zones are again observed, Zone A, the undisturbed parent carbide, Zone B, a region exhibiting plastic deformation and Zone C, the near surface layer of adhered 17-4 PH counterface steel. Figure 20. In detail there is more evidence of near surface texturing in this case, and Zone B, Figure 20, contains regions of significant plastic deformation with carbides strung out in the sliding direction. The preponderance of small carbides at the Zone B/Zone C interface is a consequence of the plastic deformation which breaks up the large carbides where strains are thought to be largest. There is evidence from the comparative EDX analysis that more Ti (TiC) is transferred and mixed into the adhered 17-4 PH in this case than for the glazed zone. Since only small volume fractions of TiC are involved it is not possible to quantify this analysis without alternative methods, however, visual confirmation of more significant

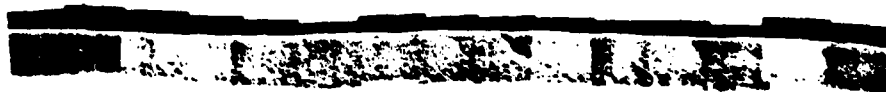


Figure 17: Montage of glazed SK wear sub-surface (x180).

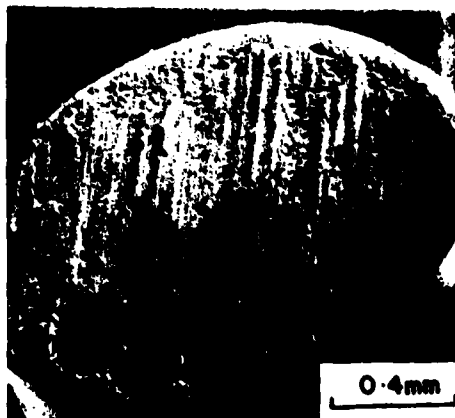


Figure 18: Wear surface of unglazed SK.



Figure 19: Montage of unglazed SK wear sub-surface (x180).

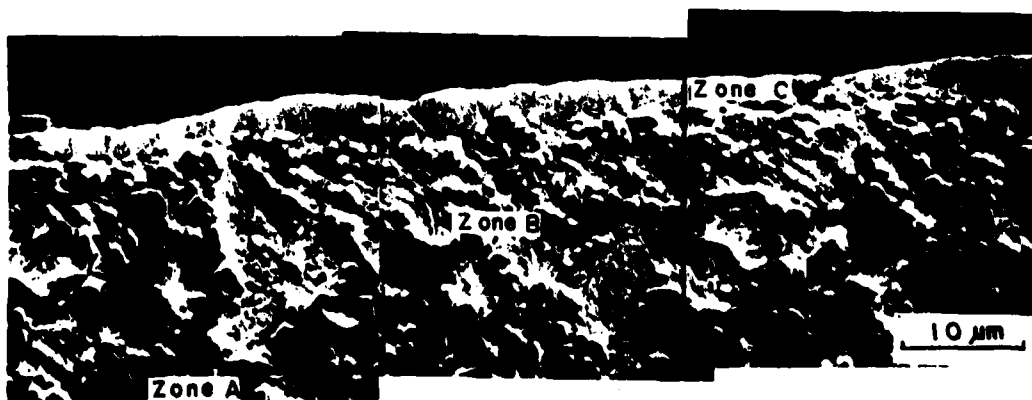


Figure 20: High magnification SEM micrograph of unglazed SK wear sub-surface. Note three zones A, B and C and the absence of sub-surface cracks.

carbide loss in the second test is given in Figure 20 where carbides are clearly present in the near surface layer.

It is clear that more severe wear occurs in the case of conventionally treated SK Ferro-TiC tool steel than for the glazed steel, however, the cracks that persist in as glazed and wear tested structures are a problem that must be overcome.

#### 5. Conclusions

- (i) Reproducible subsurface microstructure can be routinely produced for wear testing using electron-beam surface glazing techniques.
- (ii) Compound impact wear tests have been performed on area glazed M2 tool steel and SK Ferro-TiC cemented carbide (36 Vol% TiC in a tool steel matrix) with the following results:
  - (a) As glazed M2 tool steel does not wear significantly but does develop regularly spaced cracks through the glazed zone. The cracks are attributed to the brittle nature of the untempered glazed zone.
  - (b) As glazed SK Ferro-TiC wears less severely than conventionally treated SK but, as above, develops cracks through the melt quenched zone. The cracks are both trans-carbide and inter-dendritic and again can be attributed to the reaction of the brittle quench zones to the solidification rate and wear test induced strains.

#### 6. Future Work

This initial work indicates that melt quenching of Ferro-TiC tool steel modifies their subsequent wear behavior. Although this modification may be viewed as an improvement in that the effect of glazing is to reduce surface erosion during the wear test, all as glazed structures (M2 or SK) develop cracks. It is proposed that the brittle nature of untempered martensite and quenched in strains are responsible for the development of the cracks. Future tests will be performed on structures tempered for successively longer periods

of time to attempt to retain the improvement in material transport whilst avoiding zone fracture. Wear tests will also be carried out at varying loads and cycles in order to establish whether different mechanisms of wear become predominant in different loading regimes and to evaluate their interaction with the conventional and rapidly quenched microstructures.

**\*Acknowledgements**

We would like to express our thanks to Professor S. L. Rice and S.F. Wayne for their assistance in performing the wear tests.

SECTION IV

Elevation and Depression of the  $M_s$  Temperature by  
Laser and Electron Beam Glazing of a High Carbon-Low Alloy Steel

The extension of solubility limits is one important aspect of rapid quenching techniques such as laser/electron beam surface melting. As a consequence of this it is thus interesting to examine the effect of rapidly quenching steels with a higher carbon content than normally encountered. The material selected has a nominal composition of 1.5 wt%C, 1.5 wt%Cr, 0.5 wt%Mn, 0.15 Si, balance Fe and may be made superplastic by thermo-mechanically processing in the temperature range 650-1100°C. The microstructure prior to glazing consisted of fine ferrite with elongated cementite particles along the rolling direction, see Fig. 1. In this condition the microhardness is 380-400 V.H.N. Following austenitizing treatment and quenching a martensitic structure is formed with an  $M_s$  temperature of about -60°C.

To compare the effect both of laser and electron beam glazing the material the process parameters were adjusted so that a nearly identical melt depth was obtained for the same beam velocity. The CO<sub>2</sub> laser beam of 0.5mm diameter and the electron beam of 0.35mm diameter had a power of 5.1 kW and 375 watts respectively. Glazing experiments were carried out over the velocity range 0.5 to 125 cm.s<sup>-1</sup> which corresponds to an interaction time range of  $4 \times 10^{-4}$  to  $10^{-1}$ s.

In considering the laser, a hardness of 350 V.H.N. is obtained at the longest interaction time ( $10^{-2}$ s) for which a low magnification micrograph of the melt zone is shown in Fig. 2. In this dendritic structure the columnar grains are closely aligned along the radial heat flow directions. Upon subsequent quenching into liquid nitrogen the austenite in the zone transforms

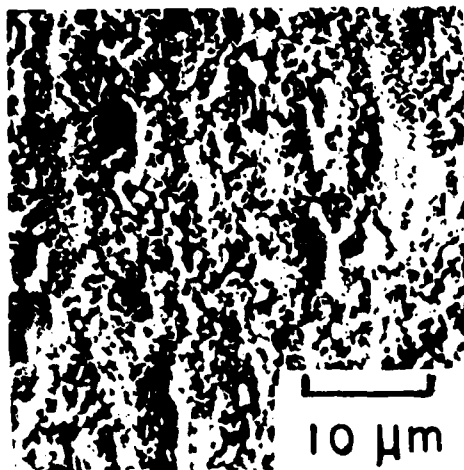


Fig. 1

Parent high carbon low alloy steel following thermomechanical treatment. Note: Carbides strung out in the rolling direction.



Fig. 2

Schematic diagram showing the microstructure of the deep penetration melting pass ( $5 \text{ cm.s}^{-1}$ )

into martensite to produce a microhardness of  $\sim 880$  V.H.N. An intriguing effect in Fig. 3 however, is the progressively increasing hardness with decreasing interaction time. At an interaction time of  $2 \times 10^{-3}$  s a well-developed martensitic structure is clearly evident in the as-glazed condition (see Fig. 4b) and as shown in Fig. 3 the microhardness is 730 V.H.N. This is an extremely intriguing result since the normal  $M_s$  temperature for this material is about  $-60^\circ\text{C}$ . With shorter interaction times the hardness decreases to a limiting value of about 950 V.H.N., see Fig. 3. At the shortest interaction time, namely  $4 \times 10^{-4}$  s, the microstructure is particularly unusual and as seen in Fig. 4a consists of an ultra fine-scale martensite with a highly convoluted appearance.

In rather striking contrast to a previous conclusion (1) the microstructural characteristics produced by laser and electron beam glazing differ appreciably. This is readily seen from the microhardness vs. interaction time curve for electron beam glazing in Fig. 3. Only at the lowest interaction time is an essentially similar result obtained with the laser and electron beam. In each case the general appearance of the entire melt zone is similar, i.e. with a strong alignment of columnar grains along radial heat flow directions. The heat distribution in the central region of the melt evidently differs, since in the electron beam melted specimen equiaxed grains form in this sections. As shown in Fig. 3, the microhardness of the electron beam melted zone is slightly higher, i.e.  $\sim 430$  V.H.N. compared with  $\sim 350$  V.H.N. The hardness of the essentially austenitic microstructure increases to  $\sim 800$  V.H.N. upon subsequent quenching into liquid nitrogen to produce a martensitic structure.

The important feature however, in surface melting with the electron beam is the slight progressive decrease in microhardness with using shorter interaction times, see Fig. 3. Thus, at the shortest interaction time ( $4 \times 10^{-4}$  s)

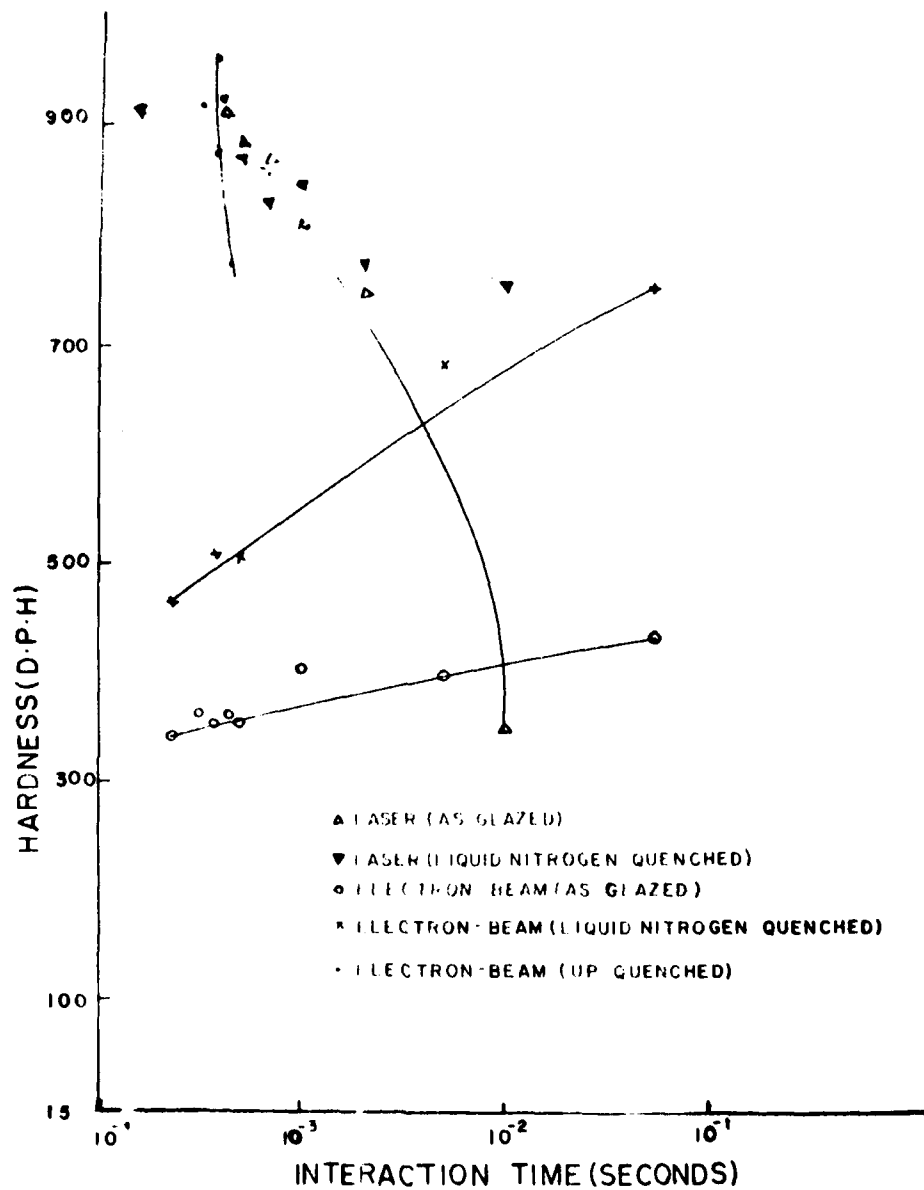


Fig Average hardness values in the melt zone as a function of interaction time.

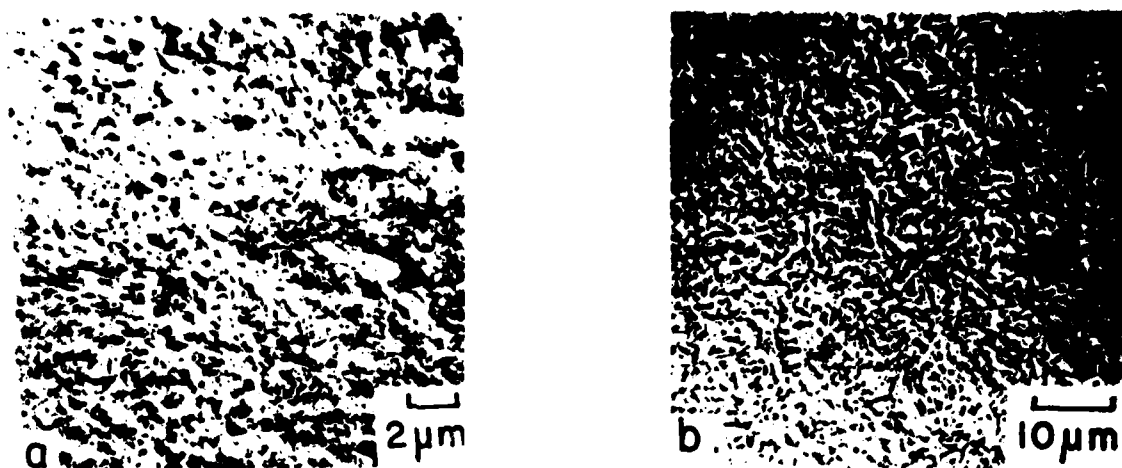


Fig. 4 Microstructure corresponding to high beam velocities. ( $125\text{ cms.s}^{-1}$  and  $25\text{ cms.s}^{-1}$ ). a) Extremely fine martensite, b) clear martensitic structure corresponding to a velocity of  $25\text{ cms.s}^{-1}$ .

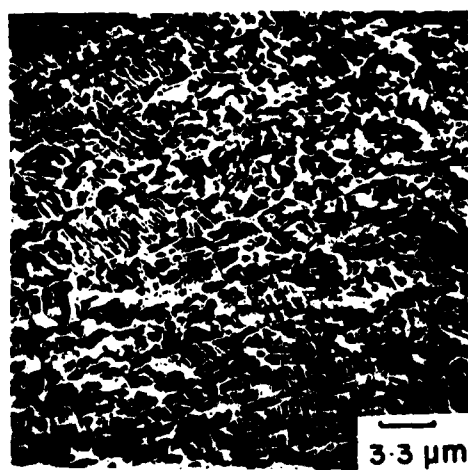


Fig. 5 Evidence of a martensitic structure obtained in the melt zone by glazing and subsequent up-quenching.

the as-glazed microhardness is  $\sim 350$  V.H.N. as compared with that of  $\sim 950$  V.H.N. for laser surface melting. Microstructural examination reveals only isolated martensite platelets and upon quenching into liquid nitrogen (or even liquid helium) the hardness only increases to  $\sim 400$  V.H.N. The intriguing feature is that optimum hardness ( $\sim 950$  V.H.N.) may be obtained in up-quenching as-glazed material. This is achieved by placing in a  $500^{\circ}\text{C}$  furnace for  $\sim 5$  minutes and cooling to room temperature. In the micrograph in Fig. 5, the well developed martensitic microstructure is clearly evident.

The underlying cause for the difference in the results obtained using a laser and electron beam as an irradiation source is highly intriguing. Particularly since a detailed study (1) has shown that comparable process parameters (such as cooling rate) are obtained when the beam power is adjusted so that an identical melt zone geometry is obtained for the same beam diameter and velocity. Accepting this, the only difference would be the nature of the environment. With laser melting noticeable surface contamination occurred even though the processing was carried out in a hood with a directed jet of argon. The electron beam, on the other hand, was carried out in a vacuum of  $\sim 10^{-5}$  torr, and the glazed surface had a mirror-like appearance.

On the basis of the preceding considerations, it would seem that oxide particles formed by surface melting with the laser play an important role. This is consistent with the concept that such particles, or precipitates act as martensite platelet nucleation sites (2-6). In the case of laser melting the strain fields set-up around oxide inclusions during cooling down in the solid state provide the driving force necessary for the formation of martensite. This apparently occurs substantially above the normal  $M_s$  temperature and to a degree that the microhardness may reach 950 V.H.N. In the case of electron beam surface melting in vacuum, contamination is reduced to the extent that insufficient nucleation sites are provided. Furthermore, with the large amount of carbon in solid solution (in the austenite) there are insufficient

carbide particle nuclei for appreciable martensite transformation even in quenching into liquid nitrogen. However, in a short duration up-quench to 500°C diffusion is sufficient to provide the requisite number of nuclei for nearly complete martensitic transformation.

Although the explanation suggested is highly tentative it is consistent with the concept that martensite is nucleated by small precipitates and inclusions. The real facination really resides in the fact that the formation and distribution of the nuclei can be varied to a considerable degree. Thus, in one case, the apparent  $M_s$  temperature is substantially increased, this is with laser melting in an air/argon atamosphere. In the other case, however, the apparent  $M_s$  temperature is reduced and, in fact,  $M_s$  is only attained by up-quenching to provide the requisite density of nuclei.

#### References


1. P. Strutt, Mat. Sci. & Eng., July, 1980.
2. M. Cohen, Met. Trans., 3, 1095, (1972).
3. R. Brook & A.R. Entwisle, J. Iron & Steel Inst., 203, 905 (1965).
4. A.R. Entwisle, Met. Trans., 2, 2395, (1971).
5. J.M. Galligan & T.J. Garosshen, Nature, 274 664 (1978).
6. M. Suezawa & H.E. Cook, Acta. Met., 28, 423 (1980).

REPORT DOCUMENTATION PAGE		READ INSTRUCTIONS BEFORE COMPLETING FORM
1. REPORT NUMBER	2. GOVT ACCESSION NO.	3. RECIPIENT'S CATALOG NUMBER
	AD-A089	637
4. TITLE (and Subtitle)		5. TYPE OF REPORT & PERIOD COVERED
Electron Beam/Laser Glazing of Iron-Base Materials		Annual Progress Report July 1980
6. PERFORMING ORG. REPORT NUMBER		
7. AUTHOR(s)		8. CONTRACT OR GRANT NUMBER(s)
Peter R./Strutt		N00014-78-C-0580
9. PERFORMING ORGANIZATION NAME AND ADDRESS		10. PROGRAM ELEMENT, PROJECT, TASK AREA & WORK UNIT NUMBERS
Metallurgy Department University of Connecticut Storrs, CT 06268		13 1766
11. CONTROLLING OFFICE NAME AND ADDRESS		12. REPORT DATE
Office of Naval Research Arlington, Virginia 22217		July 1980
14. MONITORING AGENCY NAME & ADDRESS (if different from Controlling Office)		13. NUMBER OF PAGES
		15. SECURITY CLASS. (of this report)
		Unclassified
		15a. DECLASSIFICATION/DOWNGRADING SCHEDULE
16. DISTRIBUTION STATEMENT (of this Report)		
Unlimited		
17. DISTRIBUTION STATEMENT (of the abstract entered in Block 20, if different from Report)		
18. SUPPLEMENTARY NOTES		
19. KEY WORDS (Continue on reverse side if necessary and identify by block number)		
20. ABSTRACT (Continue on reverse side if necessary and identify by block number)		
<p>The development of a programmable scanning system on an electron beam surface melting unit makes it possible to produce a rapidly quenched surface layer on a substrate material. This capability facilitates a fuller characterization of electron beam 'glazed' hard iron-base materials which include M2 tool steel and several alloyed steels dispersion strengthened with titanium carbides particles. These latter materials following 'glazing' treatment exhibit ultra-refinement of the microstructure and microhardness values well in excess of those normally obtained. Preliminary sliding/impact wear studies indicate that relatively thin</p>		

APPROXIMATELY 50 MICRO METERS

SECURITY CLASSIFICATION OF THIS PAGE(When Data Entered)

(~50  $\mu\text{m}$ ) "glazed layers" reduce surface erosion, however, isolated cracks form at periodic intervals across the surface. Finally, in a high carbon - low alloy steel "laser-glazing" and "E.B.-glazing" produced, in some instances, strikingly different microstructures and correspondingly different microhardness values. It is proposed that the nature of the "glazing" atmosphere contributes to this effect. The results are consistently interpreted on the basis of the nucleation of martensite by either small oxide or carbide particles.



SECURITY CLASSIFICATION OF THIS PAGE(When Data Entered)

## **INSTITUTE OF MATERIALS SCIENCE**

The Institute of Materials Science (IMS) was established at The University of Connecticut in 1966 in order to promote academic research programs in materials science. To provide requisite research laboratories and equipment, the State of Connecticut appropriated \$5,000,000, which was augmented by over \$2,000,000 in federal grants. To operate the Institute, the State Legislature appropriates over \$500,000 annually for faculty and staff salaries, supplies and commodities, and supporting facilities such as an electronics shop, instrument shop, a reading room, etc. This core funding has enabled IMS to attract over \$2,500,000 annually in direct grants from federal agencies and industrial sponsors.

IMS fosters interdisciplinary graduate programs in Alloy Science, Biomaterials, Corrosion Science, Crystal Science, Metallurgy, and Polymer Science. These programs are directed toward training graduate students while advancing the frontiers of knowledge and meeting current and long-range needs of our state and our nation.